State of Oregon
Oregon Department of Geology and Mineral Industries
Ruarri J. Day-Stirrat, State Geologist

OPEN-FILE REPORT O-25-02

ECOLA STATE PARK LANDSLIDE RISK ANALYSIS, CLATSOP COUNTY, OREGON

by William J. Burns[1], Laura L.S. Gabel[2], Robert W. Hairston-Porter[3], Jonathan C. Allan[2], Reed J. Burgette[1], Jon J. Franczyk[1], Lowell H. Anthony[1], Jason D. McClaughry[1,4], and Alan R. Niem[5]

2025

[1]Oregon Department of Geology and Mineral Industries, 800 NE Oregon Street, Suite 965, Portland, OR 97232
[2]Oregon Department of Geology and Mineral Industries, Coastal Field Office, P.O. Box 1033, Newport, OR 97365
[3]Formerly at Oregon Department of Geology and Mineral Industries, 800 NE Oregon Street, Suite 965, Portland, OR 97232
Presently at U.S. Geological Survey, 1819 SW 5th Ave, Portland, OR 97201
[4]Oregon Department of Geology and Mineral Industries, Baker City Field Office, 1995 3rd Street, Suite 130, Baker City, OR 97814
[5]Emeritus, College of Earth Ocean and Atmospheric Sciences, Oregon State University, 104 CEOAS Administration Building, Corvallis, Oregon 97331-5503

DISCLAIMER

This product is for informational purposes and may not have been prepared for or be suitable for legal, engineering, or surveying purposes. Users of this information should review or consult the primary data and information sources to ascertain the usability of the information. This publication cannot substitute for site-specific investigations by qualified practitioners. Site-specific data may give results that differ from the results shown in the publication.

WHAT IS IN THIS REPORT?

This paper evaluates landslide hazard and risk at Ecola State Park, Clatsop County, Oregon. The intended audiences for this paper include those in government, industry, academia, and the public.

Cover Image: Oblique Digital Elevation Model (DEM) image of the southern portion of Ecola State Park. Image credit: Jon Franczyk

Expires: 1/1/2026

Oregon Department of Geology and Mineral Industries Open-File Report O-25-02
Published in conformance with ORS 516.030

For additional information:
Administrative Offices
800 NE Oregon Street, Suite 965
Portland, OR 97232
Telephone (971) 673-1555
https://oregon.gov/DOGAMI/

TABLE OF CONTENTS

LIST OF FIGURES

LIST OF TABLES

LIST OF MAP PLATES

See the digital publication folder for files.

Plate 1. Map of the Ecola State Park Study Area
Plate 2. Geologic Map of the Ecola State Park Study Area
Plate 3. Lidar-Based Regional Landslide Inventory Map of the Ecola State Park Study Area
Plate 4. Serial Orthophoto-Based Landslide Inventory Map (1939-2022) of the Ecola State Park Study Area
Plate 5. Serial Lidar-Based Landslide Inventory Map (2009-2023) of the Ecola State Park Study Area
Plate 6. Landslide Susceptibility and Risk Map of the Ecola State Park Study Area

GEOGRAPHIC INFORMATION SYSTEM (GIS) DATA

See the digital publication folder for files.
Metadata is embedded in the geodatabase and is also provided as separate.xml format files.

O-25-02_EcolaLandslideRisk.gdb:

Feature dataset: SP-42_LandslideInventory

Feature classes:

SP-42 Landslide Inventory Deposits (polygon)
SP-42 Landslide Inventory Scarp_Flanks (polygon)
SP-42 Landslide Inventory Scarps (polyline)

Feature dataset: GeologicMap

ContactsAndFaults (polylines)
MapUnitPolys (polygon)
Orientations (points)

Raster dataset: Landslide Susceptibility and Risk Map

Feature datasets:

LidarChange_LandslideInventory_2009_2023 (polygon)
Study_Area (polygon)
Orthophoto_LandslideInventory (polygon)

UNITS OF MEASUREMENTS

The intended audience for this report includes Oregon State Parks staff and government, industry, academia, and the public. Therefore, we selected U.S. Customary units as the primary units. A conversion table for U.S. Customary units to SI (International System) Metric units is included for easier conversion where needed.

SI Metric Units to U.S. Customary Units

	Multiply	By	To obtain
length:	millimeter (mm)	0.039	inch (in)
	centimeter (cm)	0.394	inch (in)
	meter (m)	3.281	foot (ft)
	meter (m)	1.094	yard (yd)
	kilometer (km)	0.621	mile (mi)
area:	square kilometer (km^2)	0.386	square mile (mi^2)
volume:	cubic meter (m^3)	35.315	cubic ft (ft^3)
	cubic meter (m^3)	1.308	cubic yard (yd^3)
	cubic kilometer (km^3)	0.240	cubic mile (mi^3)

U.S. Customary Units to SI Metric Units

	Multiply	By	To obtain
length:	inch (in)	25.4	millimeter (mm)
	inch (in)	2.54	centimeter (cm)
	foot (ft)	0.305	meter (m)
	yard (yd)	0.914	meter (m)
	mile (mi)	1.609	kilometer (km)
area:	square mile (mi^2)	2.590	square kilometer (km^2)
volume:	cubic ft (ft^3)	0.028	cubic meter (m^3)
	cubic yard (yd^3)	0.765	cubic meter (m^3)
	cubic mile (mi^3)	4.168	cubic kilometer (km^3)

EXECUTIVE SUMMARY

Oregon's state parks are treasures that make Oregon an ideal place to live and explore. Ecola State Park (Ecola) is located on the northern Oregon Coast in Clatsop County between the cities of Seaside and Cannon Beach. Landslide hazards have been an issue at Ecola since its designation in 1932.

The purpose of this project is to evaluate the current and future landslide susceptibility and risk within and surrounding Ecola to assist the Oregon Parks and Recreation Department (OPRD) in making decisions to reduce landslide risk, with an emphasis on roadways. Landslide susceptibility is the relative likelihood of the landslide hazard occurring in a certain portion of the study area. Landslide risk is the possibility of damage or losses to assets (people, infrastructure, and the environment) by the hazard. To accomplish this goal, several tasks were performed:

- A new lidar topography dataset was collected in 2023.
- The distribution of landslides was mapped throughout the park.
- A new/updated geologic map of the park was created.
- Existing and future landslide susceptibility was analyzed.
- Recommendations for future risk reduction were provided.

Landslide susceptibility and risk were analyzed using several methods, including:

- Landslide inventory: an inventory of contemporary and historic landslide activity was created by examining the 2023 topographic lidar dataset.
- Serial lidar change analysis: landslide activity was identified by examining changes in the topography during a window of time using lidar datasets (2023 and 2009).
- Serial orthophoto change analysis: landslide activity was identified by examining changes in the vegetation and other visual details using multiple orthorectified aerial images spanning 1939 to 2022.
- Geologic mapping: geologic mapping data from the region was collected, corroborated and further investigated with several field days during this study, and combined to build a robust geologic map that can be used in the development of a landslide susceptibility map and provide additional understanding of landslide mechanisms.

Finally, landslide inventories, geologic mapping data, and modern topography were combined to create a susceptibility and risk map that classifies every portion of the study area into one of the seven susceptibility zones, from *None* to *Low* to *Active* susceptibility of future landslide activity and risk of damage and losses to existing infrastructure. Each zone includes an estimate of past landslide-recurrence activity (e.g., every ~50 years to 150 years) and recommendations for future development to reduce risk.

1.0 BACKGROUND

Oregon's state parks are treasures that make Oregon an ideal place to live and explore. Ecola State Park (herein referred to as Ecola) is located on the northern Oregon Coast in Clatsop County between the cities of Seaside and Cannon Beach (**Figure 1-1;** Plate 1). The park stretches along nine miles of the rocky Pacific Ocean coastline known as Tillamook Head. The park offers opportunities for outdoor recreation, including hiking, picnicking, tide pool exploration, surfing, and wildlife observation. Given its proximity to neighboring coastal towns and to Portland, Ecola is one of the most popular day-use parks on the coast, averaging 526,000 (±92,000) visitors per year (Cox, B., written communication, October 2024). However, in recent years use of the park during the winter has been limited due to active landsliding that periodically cuts off the primary access road. For example, visitor numbers decreased by 200,000 and 270,000 people in 2022 and 2023, respectively, due to road closures.

Figure 1-1. Map of Clatsop County and the study area.

Part of the reason Oregon State Parks are so unique and beautiful is the underlying geology. However, with beauty and dynamic landscapes often comes natural hazards. Landslide hazards have been an issue at Ecola since its designation in 1939. The purpose of this project is to evaluate the current and future landslide susceptibility and risk within and surrounding Ecola to assist the OPRD in making decisions to reduce landslide risk, with an emphasis on roadways. Landslide susceptibility is the relative likelihood of the landslide hazard occurring in a certain portion of the study area. Landslide risk is the possibility of

damage or losses to assets (people, infrastructure, and the environment) by the hazard. To accomplish this goal, several tasks were completed:

- A new lidar topography dataset was collected in 2023;
- Landslides were mapped throughout the park;
- An updated geologic map of the park was made;
- Existing and future landslide susceptibility was analyzed; and,
- Recommendations for future risk reduction were determined.

Landslide susceptibility and risk were evaluated using several methods, including:

- Geologic Mapping: A geologic map for the park was made based on geologic mapping by Niem and others (unpublished data, 2024; Plate 2) that was used to better understand landslide mechanisms and to develop a landslide susceptibility map.
- Landslide Inventory: An inventory of prehistoric and historic landslide activity was created by Burns and others (2021) and updated with the 2023 topographic lidar dataset (Plate 3).
- Aerial Photograph-Based Change Analysis: Landslide activity by was identified by examining changes in the vegetation and other visual details using multiple orthorectified aerial images spanning 1939–2022 (Plate 4).
- Lidar-based Change Analysis: Landslide activity was identified by comparing topographic changes between the 2009 and 2023 lidar datasets (Plate 5).
- Landslide Susceptibility: Landslide Inventories, geologic mapping, and lidar topography datasets were combined to create a susceptibility and risk map. This map classifies every portion of the study area into one of the seven zones, from *Low* to *High* risk of future landslide activity. Each zone provides an estimate of when future landslide activity may occur (e.g., every ~50 to 150 years) and gives recommendations for future development (Plate 6).

The northern Oregon Coast temperate climate is mild and cool with warm, dry summers and moderately cool, wet winters. Normal annual precipitation is between 65 in–90 in with most precipitation occurring during the winter months (typically October through March; **Figure 1-2**). The frequent low-to-moderate-intensity drizzle is interrupted by high-intensity atmospheric river (AR) storms that can last several days and deliver 4 in–8 in of rain in a 24-hour period (NWS, Public Information Statement, December 4, 2007; Shaefer and others, 2008).

The topography of Ecola is mountainous with minimal flat land. Elevations range from sea level to a maximum of 1,155 ft along the northern side of Tillamook Head (Plate 1). The slopes are mostly moderate, ranging from 0°30°, but can be very steep (45°+) along the ocean cliffs. Because of the park's unique geology and terrain, the park has been subject to landslide hazards since its formation in 1939.

Figure 1-2. Map of the mean annual precipitation in Oregon. Ecola (black box on map) is located on the northern Oregon Coast, which receives greater than 100 in of precipitation per year (Copyright ©2022, PRISM Climate Group, Oregon State University, https://prism.oregonstate.edu, map created 2022).

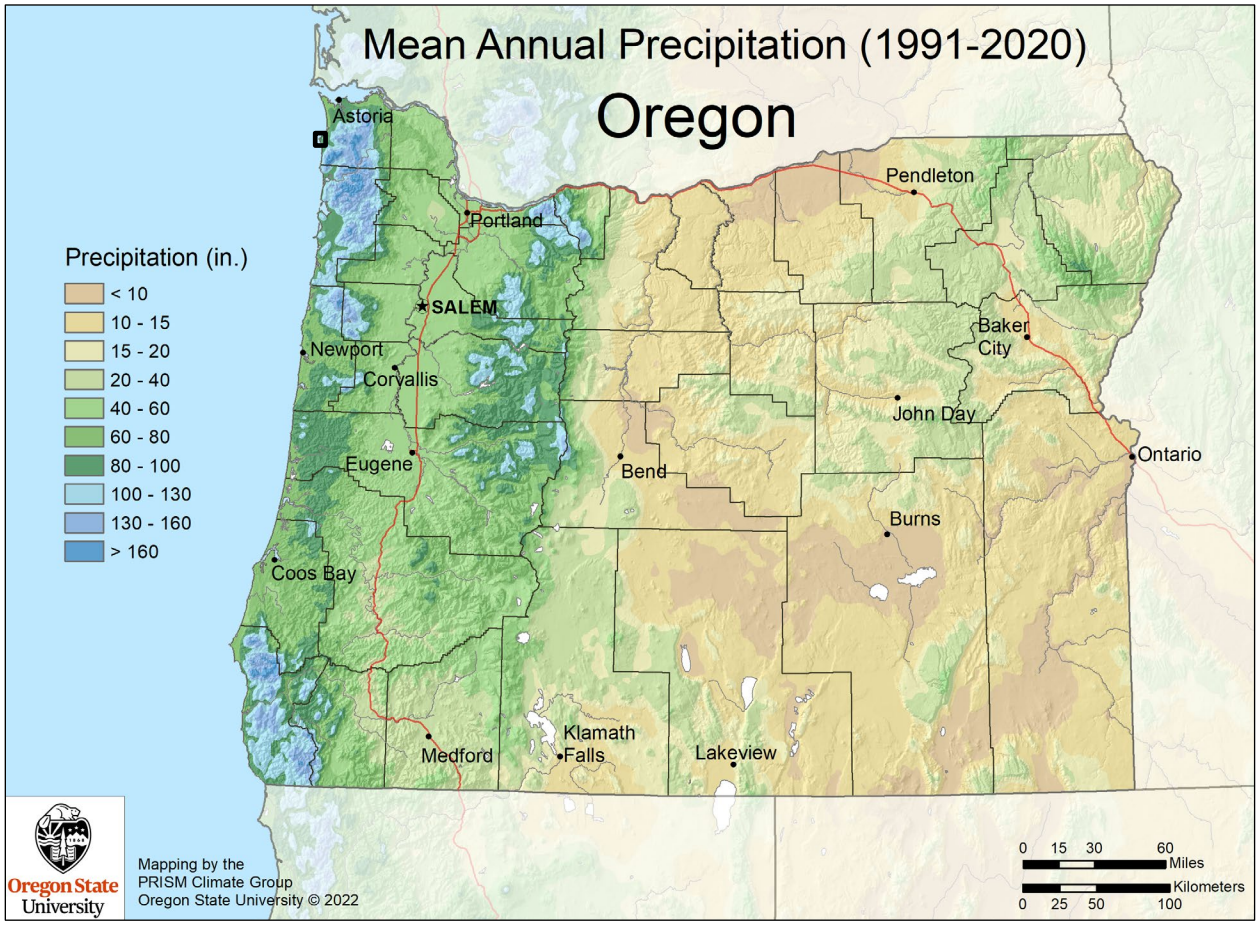

1.1 History of the Park

On January 8, 1806, Captain William Clark of the Lewis and Clark Expedition was looking south from Tillamook Head and described the view as the *"grandest and most pleasing prospect he had ever surveyed."* (Lewis and Clark, 1806). The land that makes up Ecola was acquired by the State of Oregon between 1932 and 1978 by gift and purchase from private owners and the federal government. The original tract was 451 acres at the south end of modern Ecola, near Cannon Beach (Plate 1). Later, additional land was acquired to the north and east, including Tillamook Head and extending to Seaside. Ecola was developed between 1934 and 1941, with construction of roads, picnic facilities, trails, offices, workshop and a caretaker's house (https://stateparks.oregon.gov/).

Ecola is located very close to the intersection of Oregon State Highways 26 and 101 in Clatsop County (**Figure 1-3;** Plate 1). Ecola is directly adjacent to Elmer Feldenheimer State Natural Area (east of Ecola), which is currently undeveloped. This project's study area includes both OPRD properties as well as a portion of private land between the state lands and Highway 101 (**Figure 1-3;** Plate 1).

Figure 1-3. Map of Ecola and this study's area. Ecola is adjacent to Elmer Feldenheimer State Natural Area to the east and John Yeon State Natural Site to the south.

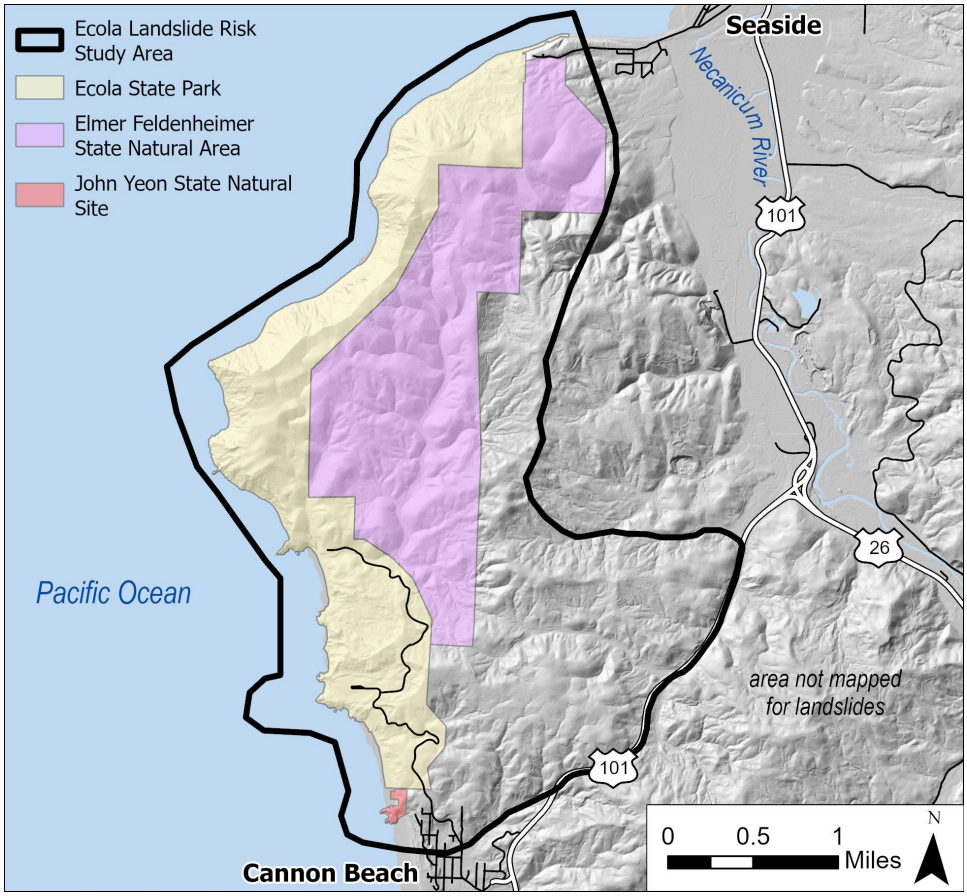

1.2 Geology

The geology of Ecola and the surrounding region has been studied and mapped by Schlicker and others (1961), North and Byrne (1965), Schlicker and others (1972), Niem and others (1973, 1990, 1994), Niem (1975), Carson and Hankel (1975), Neel (1976), Niem and Niem (1985), and Witter and others (2009). Many of these publications also discussed landslide hazards. New detailed geologic mapping in the region by Niem and others (unpublished data, 2024) updates the geologic framework for the area and serves as a basis for landslide analysis in this study (Plate 2).

All of the geology in Oregon stems from the position on an active plate margin between the overriding North American Plate and the subducting Pacific Plate (Madin, 2009). The geologic setting is commonly referred to as the Cascadia Subduction Zone (CSZ), where the Juan De Fuca Plate is subducting beneath Oregon and the Pacific Northwest (Madin, 2009). The CSZ can produce 9+ magnitude earthquakes, and the last one occurred on January 26, 1700 (**Figure 1-4**; Atwater and others, 2005). The next rupture of the CSZ is anticipated to cause widespread destruction throughout the Pacific Northwest, including thousands of landslides and a tsunami along the coast. We expect many existing landslides along the Oregon Coast to be triggered and move in the next CSZ major earthquake.

Figure 1-4. Map of perceived shaking and damage potential from a CSZ earthquake (Madin and others, 2021). The study area is outlined by a black box on the map. Hotter colors (red, orange, yellow) indicate higher shaking and damage potential. Cooler colors (green and blue) indicate lower shaking and damage potential.

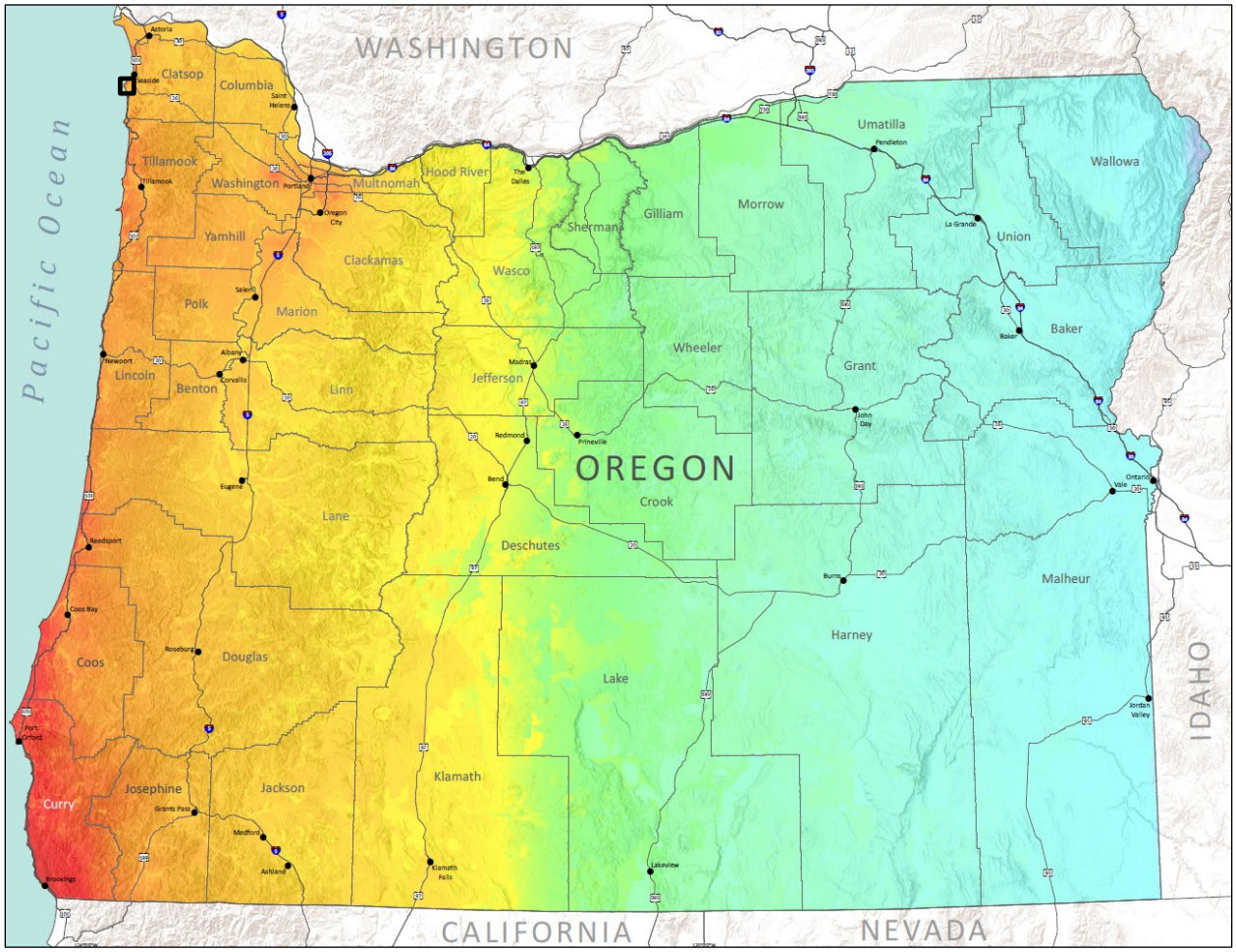

In general, the geology of Ecola consists of three primary bedrock units: the Oligocene Smuggler Cove Formation (**Tsc**), lower Miocene Astoria Formation (**Tac**, **Tac1**), and lower Miocene Columbia River Basalt Group (CRBG; **Tgww**, **Tgwws**, **Tgwwd**, **Tgsbi**, **Twfgi**)(Plate 2). Quaternary sediments deposited on top of bedrock formations include: Upper Pleistocene and Holocene coastal-fluvial terrace deposits (**Qpt**, **Qft**), Holocene fluvial and estuarine deposits (**Qal**) along streams, Holocene dune sand (**Qds**), and Holocene beach deposits (**Qbs**, **Qbd**).

The oldest geologic unit in Ecola, cropping out only in the northern part of the park, is the Oligocene Smuggler Cove Formation (**Tsc**; Neel, 1976; Niem and Niem, 1985). This sequence of tuffaceous bioturbated claystone and tuffaceous muddy siltstone was deposited in a deepwater bathyal environment (Cressy, 1974; Niem and Cressy, 1973; Niem and Niem, 1985; Niem and others, 1994).

The Astoria Formation (**Tac**, **Tac1**) is a widespread, scattered coastal litho-stratigraphic unit exposed in four sedimentary basins from Astoria to Newport, Oregon (Snavely and others, 1976) and in southwest Washington (Wolfe and McKee, 1968). The Cannon Beach Member is the only part of the Astoria Formation mapped in Ecola, where it disconformably overlies the Oligocene Smuggler Cove Formation (**Tsc**). This sequence of well-laminated, dark-gray, micromicaceous and carbonaceous mudstone (**Tac**) and fine-grained quartzo-feldspathic turbidite sandstone (**Tac1**) was deposited in a calm deep-marine

depositional environment (anoxic to burrowing organisms) on the upper continental slope or outer-shelf (Rau in Niem and others, 1973; Niem and others, 1994, unpublished data, 2024).

Sedimentary rock units in Ecola are intruded by invasive lava flows of the CRBG (**Tgww**, **Tgwws**, **Tgwwd**, **Tgsbi**, **Twfgi**; Niem and Cressy, 1973). The CRBG is an extensive succession of lower Miocene tholeiitic basalt and basaltic andesite lava flows that cover more than 130,488 mi^2 in parts of Washington, Oregon, and Idaho. These lava flows largely erupted from NNW-striking linear fissure systems in the eastern part of the Columbia Plateau between 16.2 and 15.9 million years ago and flowed west through the Columbia trans-arc lowland to the Miocene Pacific coastline of Oregon and Washington (Wells and others, 2009; Camp and Wells, 2021). When some lava flows reached the early Miocene Pacific Ocean, they formed westward-inclined foreset-bedded lava deltas above older marine sediments (Wells and others, 2009). Relatively dense lava flows invaded soft, water-saturated, semi-consolidated deep-marine sediments of the Astoria Formation, forming a complex network of sills, dikes, and irregularly shaped invasive intrusive bodies (Schlicker and others, 1961; Niem and Cressy, 1973; Niem and others, unpublished data, 2024). Pervasive invasion of the lava flow bodies into the marine sediment was accompanied by formation of basalt breccia and peperitic contacts, complex deformation (chevron folding) of the sediments, and local hydrothermal contact baking metamorphic effects.

Most of the larger deep landslides in Ecola originate within the Cannon Beach Member of the Astoria Formation (**Tac**, **Tac1**), an overall fine-grained lithology that is characterized by weak bedding planes, relatively low material strength, and deformation by several processes. Schlicker and others (1961) proposed that deformation caused by basalt intrusions may have weakened the sedimentary rock and made them more landslide prone. About one-third of the exposed Smuggler Cove Formation in Ecola is associated with overlying basalt landslides sourced from the West Point fault scarps.

Geologic units shown on Plate 2, following the work of Niem and others (unpublished data, 2024), are as follows:

Quaternary Surficial Deposits

Qbs **beach sand and basalt gravel berm (Holocene)—**Tan to brown, moderately well sorted, fine- to medium-grained sand composed predominantly of subrounded to subangular grains of quartz, feldspar, mica, and basalt. The sand includes parallel laminae and micro cross-ripple laminae of very-fine, well-sorted heavy minerals, mainly black magnetite/ilmenite, dark green pyroxene, zircons, and reddish garnets. Beach sand is 3 ft–6 ft thick, with overlying beach gravel and laterally higher gravel berms. Gravel berms are medium-gray with moderately sorted, subrounded to well-rounded, subspherical to landward imbricated disc-shaped basalt pebbles and cobbles. Logs stripped of bark and limbs, smoothed by wave abrasion top, beach sand and gravel berms near the base of sea cliffs and at the mouths of streams.

Qbg **basalt beach gravel (Holocene)—**Medium-gray, loosely consolidated, moderately sorted and thick-bedded, framework-supported gravels containing well-rounded to subangular, hard, tabular to disc-shaped polished boulders (up to 3 ft), cobbles, and some pebbles of medium-gray. Gravel deposits are several feet thick, forming reverse-graded berms in narrow arcuate pocket beaches bounded by high headlands and sea cliffs of CRBG (e.g., Tillamook Head).

Qds **dune sand (Holocene)—**Beach grass-covered, active and inactive well sorted, very-fine- to fine-grained, quartzo-feldspathic, planar to trough, crossbedded and wind ripple micro cross-

laminated dune sands present north of the mouth of Ecola Creek. Sand includes laminae with mica and thin foreset crossbedded laminae with concentrations of very fine, dark gray to black magnetite and ilmenite.

Qal **alluvium and estuarine deposits (Holocene)—**Unconsolidated deposits of poorly sorted, angular to subangular, tabular to blocky, weather-stained pale reddish to yellow-brown basalt boulders to cobbles with minor sand, silt, and clay, and organic woody debris along streams. Locally, gravels in the base of stream channels and cut banks are cemented by reddish-brown to yellowish-brown iron oxide minerals (e.g., hematite, goethite, limonite). The thickness of alluvial deposits is generally 3 ft–7 ft.

Qft **coastal and fluvial terrace deposits (Holocene and Pleistocene)—**Fluvial terrace deposits are mapped at the mouths of Indian and Cannon creeks, where the streams flow onto Indian Beach. Terrace deposits consist of 13 ft–23 ft of loosely consolidated, weathered, poorly to very poorly sorted, framework-supported gravel containing tabular, pale-yellowish-orange boulders and cobbles to rounded pebbles of Winter Water basalt (**Tgww**) and carbonized logs. Gravels include a matrix of minor, fine reddish-oxide-coated feldspar, quartz, and basalt sand and silt. Interbeds between gravel lenses are 3 ft–7 ft thick consisting of dark-gray to weathered light-brownish-yellow mud and dark-gray to black carbonaceous woody debris.

Qpt **coastal-fluvial terrace deposits (Upper Pleistocene)—**Unconsolidated to moderately consolidated gravel, beach, and dune sand; locally contains minor consolidated clay-rich paleosol, colluvium, debris flows, and alluvial sand, silt, and gravel deposited in channel and point bar environments.

Columbia River Basalt Group

Wanapum Basalt

Frenchman Springs Member

Twfgi **Basalt of Ginkgo, invasive sills and dikes (lower Miocene)—**Medium-gray to dark-gray, plagioclase microphyric and porphyritic tholeiitic basalt with large (0.2 in–1.0 in) yellow-brown to very pale orange plagioclase glomerocrysts. **Twfgi** is distinguished from older Grande Ronde Basalt by abundant large plagioclase glomerocrysts, lower SiO_2 and higher TiO_2 and P_2O_5 contents, and excursional or transitional polarity (Reidel and others, 2002; Wells and others, 1989; Tolan and others, 2009; Wells and others, 2009, 2020). In Ecola and the surrounding area, **Twfgi** forms a 33–49-ft-thick horizontal sill and an early Miocene age of ~16.1 Ma (million years ago; Kasbohm and Schoene, 2018; Baksi, 2022; Kasbohm and others, 2023). The thermal effect of sill emplacement baked both the underlying and overlying **Tac** in the north-central part of Ecola.

Grande Ronde Basalt

Normal-polarity (N2) magnetostratigraphic unit

Sentinel Bluffs Member

Tgsbi **Sentinel Bluffs Member, invasive basalt sill (lower Miocene)—**Light- to dark-gray, aphyric to sparsely plagioclase-phyric tholeiitic basalt, locally with characteristic sparse, small (<0.2 in),

tabular plagioclase phenocrysts. **Tgsbi** is distinguished from other members of the Grande Ronde Basalt by common diktytaxitic texture, higher content of MgO, and paleomagnetic directions (Wells and others, 2009). The only part of the **Tgsbi** exposed in Ecola is an invasive sill cropping out at Chapman Point and Bird Rocks in the southwest part of the study area. **Tgsbi** has an early Miocene age of ~16.1 Ma (Kasbohm and Schoene, 2018; Baksi, 2022; Kasbohm and others, 2023). **Tgsbi** is equivalent, in part, to the Sentinel Bluffs Member of Reidel and Tolan (2013).

Winter Water Member

Tgww **Winter Water Member (lower Miocene)—**Dark-gray, columnar-jointed basaltic andesite lava flows that lie above sedimentary rocks of the **Tac** and **Tac1** in Ecola. The basaltic andesite is characterized by small, euhedral, prismatic plagioclase phenocrysts and small (0.08 in) radial or spoke-shaped plagioclase glomerocrysts (Tolan and others, 2009). **Tgww** is distinguished from **Tgsbi** by higher amounts of TiO_2 and lesser amounts of MgO, and paleomagnetic directions (Wells and others, 2009). **Tgww** has an early Miocene age of ~16.2 Ma (Kasbohm and Schoene, 2018; Baksi, 2022; Kasbohm and others, 2023). **Tgww** is equivalent to the Winter Water Member of Reidel and Tolan (2013).

Throughout Ecola, unit **Tgww** is associated with compositionally indistinguishable irregular-shaped sills and dikes invasive into underlying sedimentary rocks. Subdivided to show:

Tgwws **Winter Water Member, invasive basalt sills (lower Miocene)—**Basaltic andesite horizontal to subhorizontal sills averaging 32 ft–98 ft in thickness. The largest of the sills in Ecola is the invasive ~1000-ft-thick, east-dipping sill that forms Tillamook Head (Plate 2). Locally, finger-like basalt intrusions off the top of this sill invade and intensely fold semiconsolidated sandstones and mudstones of **Tac**. Pepperite, a mixture of large and small hydrothermally altered basaltic breccia cemented by white quartz, red microcrystalline jasper, white zeolite, and calcite veins, is common along the basalt sediment contacts.

Tgwwd **Winter Water Member, invasive basalt dikes (lower Miocene)—**Basaltic andesite, vertical to subvertical dikes averaging 16 ft–32 ft in width.

Astoria Formation

Cannon Beach Member

Tac **deep marine micromicaceous mudstone (lower Miocene)—**Medium- to dark-gray, finely laminated micromicaceous mudstone, with alternating laminae of light-gray siltstone and dark-gray silty claystone (Snavely and others, 1976; Tardif, 2023). The mudstone contains bathyal foraminifera (Niem and others, 1973). Thickness of **Tac** is as much as 1968 ft. In Ecola, dark-gray mudstone is exposed in 66 ft–98-ft-high sea cliffs north and south of Bald Point; it is weathered to pale yellow-orange to yellowish-brown in the upper 33 ft of these sea cliffs. Inland, the mudstone is poorly exposed, eroding to form low, densely vegetated slopes. Where **Tac** is in contact with invasive CRBG, fresh, dark-gray mudstone is baked white and is more indurated due to the hydrothermal contact metamorphic effect (e.g., at the top of Tillamook Head). The Cannon Beach Member is subdivided in Ecola to show:

Tac1 **micaceous and carbonaceous fine-grained quartzo-feldspathic turbidite sandstone (lower Miocene)—**Nested, channelized, and rhythmically interbedded light-gray, graded, fine-grained, micaceous and carbonaceous quartzo-feldspathic volcaniclastic turbidite sandstone beds (1.6 ft–3.3 ft thick) and laminated to thin-bedded, dark-gray micromicaceous mudstone (1 ft–1.6 ft thick). Thickness of **Tac1** is as much as several hundred feet in the lower part of the Cannon Beach Member (T**ac**). **Tac1** underlies, and may interfinger with, **Tac**.

Smuggler Cove Formation

Tsc **tuffaceous and bioturbated clayey siltstone (Oligocene)—**Structureless, intensively bioturbated tuffaceous claystone and tuffaceous muddy siltstone with a few scattered graded volcanic fine-grained sandstone beds, thin, very light-gray tuffs, and green-gray glauconitic sandstone (Niem and Niem, 1985). Subunits commonly have clastic dikes and calcareous concretions. Abundant small, hook-shaped *Phycosiphon* (Helmenthoida) burrows are ubiquitous and characteristic of **Tsc**. **Tsc** is best exposed in colluvium-covered, 40-ft- to 80-ft-high sea cliffs from Surfers Beach in Seaside, south to West Point in Ecola, north of the east/southeast to west/northwest trending fault. In Ecola, the unit generally forms broad slopes and low stream-dissected hills. Thickness of **Tsc** in the area is as much as 3,280 ft.

1.3 Landslide Characteristics and Types

Landslide refers to a range of mass movements, including rockfalls/topples, channelized debris flows, slides, and other mass movements (Varnes, 1978). Different types of landslides have different frequencies of movements, different triggering conditions, and very different resulting hazards. All mass movements can be classified into four predominant types: 1) falls/topples, 2) slides, 3) spreads, 4) flows. **Figure 1-5** provides definitions of each. Most slope failures are complex combinations of these distinct types, but the generalized groupings provide a useful means for framing discussion of the type of hazard associated with the landslide, the landslide characteristics, identification methods, and potential mitigation alternatives (Burns and Madin, 2009).

Figure 1-5. Types of mass movements (Burns and Madin, 2009; Highland, 2004).

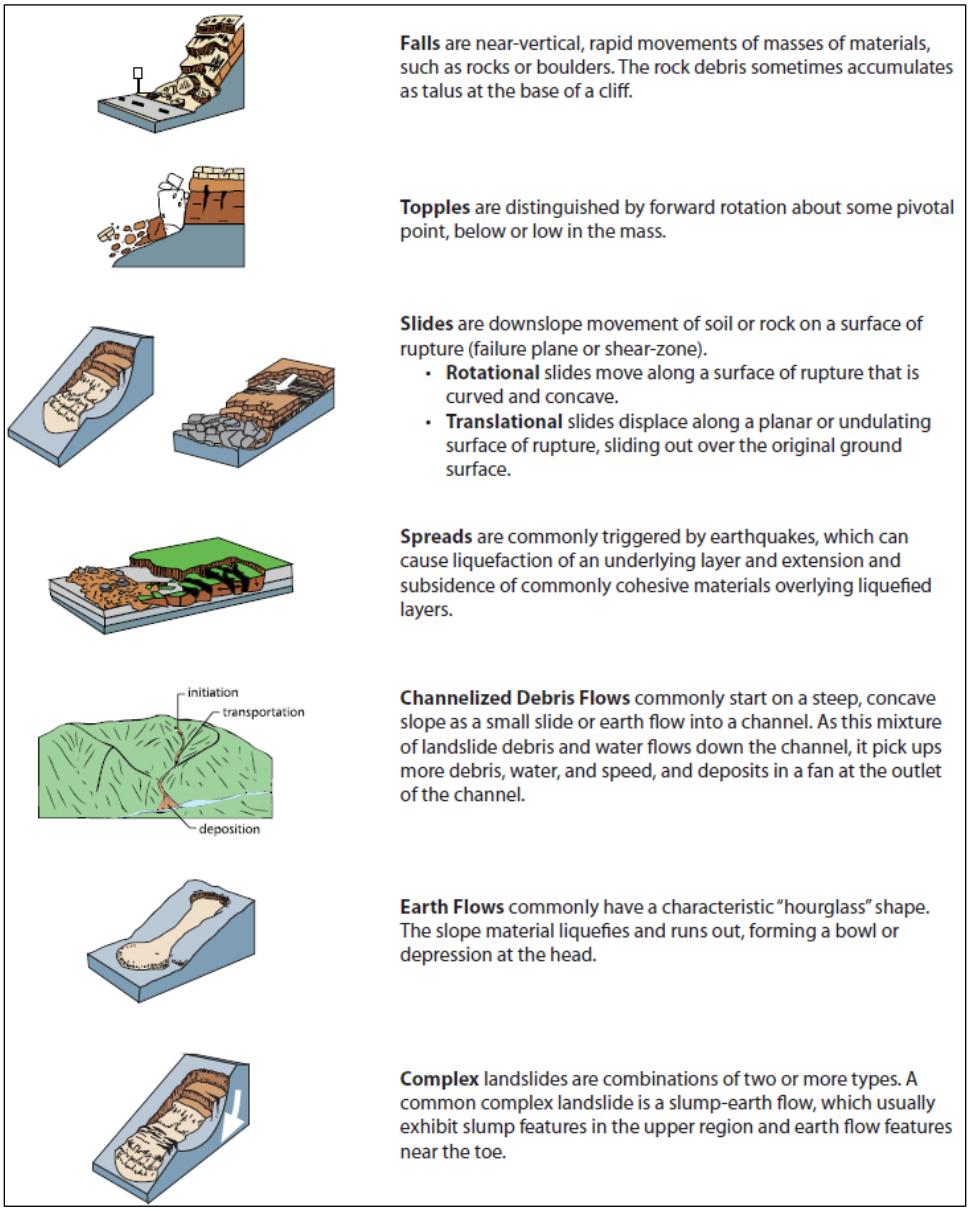

Falls are near-vertical, rapid movements of masses of materials, such as rocks or boulders. The rock debris sometimes accumulates as talus at the base of a cliff.

Topples are distinguished by forward rotation about some pivotal point, below or low in the mass.

Slides are downslope movement of soil or rock on a surface of rupture (failure plane or shear-zone).

- **Rotational** slides move along a surface of rupture that is curved and concave.
- **Translational** slides displace along a planar or undulating surface of rupture, sliding out over the original ground surface.

Spreads are commonly triggered by earthquakes, which can cause liquefaction of an underlying layer and extension and subsidence of commonly cohesive materials overlying liquefied layers.

Channelized Debris Flows commonly start on a steep, concave slope as a small slide or earth flow into a channel. As this mixture of landslide debris and water flows down the channel, it pick ups more debris, water, and speed, and deposits in a fan at the outlet of the channel.

Earth Flows commonly have a characteristic "hourglass" shape. The slope material liquefies and runs out, forming a bowl or depression at the head.

Complex landslides are combinations of two or more types. A common complex landslide is a slump-earth flow, which usually exhibit slump features in the upper region and earth flow features near the toe.

Generally, falls and topples occur in areas in Oregon with semicompetent rock like basalt, which is most commonly exposed at the surface as near-vertical cliffs and lacks soil and vegetation cover. Rock falls/topples generally occur in isolated locations because of the unique landscape conditions. The events are usually small to medium sized, but are a continuous process.

Slides, referred to as landslides for the remainder of this report, occur in Oregon in areas with relatively weak geology (meaning the bedrock is not very hard or consolidated), along contacts between weak and strong units, and/or in locations where the structural geology promotes instability (e.g., small crustal faults). Landslides are commonly divided into two types: shallow and deep. Shallow landslides have a failure surface <15 ft below the ground surface and deep landslides have a failure surface >15 ft (Burns and Madin, 2009). It is important to distinguish this difference because the level of effort required to mitigate these two types is significantly different. For example, shallow slides can commonly be mitigated using standard excavation procedures, but deep landslides commonly require much more complicated and expensive mitigation techniques.

Spreads are the least common, but when found, are almost always along a riverbank as they are usually triggered during earthquakes and caused by liquefaction of underlying materials.

Flows, which have a relatively high water content, are very common in Oregon and especially in western Oregon where there is significant precipitation. One type is the channelized debris flow, which can travel long distances and reach speeds of tens of miles per hour and is therefore life threatening. For more information about landslides see the following fact sheets:

- https://pubs.usgs.gov/fs/2004/3072/pdf/fs2004-3072.pdf
- https://pubs.oregon.gov/dogami/fs/landslide-factsheet.pdf

1.4 Previous Landslide Studies

This report discusses several distinct landslides within Ecola. These slides have been studied many times over the years, however there is some variation in how they are identified. For consistency, and to ensure all knowledge about a given feature has been recognized, Plate 3 presents a map of these slides along with the names they will be identified with for the remainder of this report. Like the geology, the landslides in Ecola and the surrounding region have been studied and mapped by several geologists and engineers, including: Schlicker and others (1961), North and Byrne (1965), Schlicker and others (1972), Carson and Hankel (1975), Witter and others (2009), Pfeiffer (2016), Wavra (2021), and Burns and others (2021).

Interestingly, the first observation of slope instability was made by Meriwether Lewis on January 10, 1806. Lewis wrote in his journal, "The coast in the neighbourhood of Clarks Mountain is sliping off & falling into the Ocean in immence masses; fifty or a hundred Acres at a time give way and a great proportion in an instant precipitated into the Ocean." (Lewis and Clark, 1806). Schlicker and others (1961) were the first to map landslides in Ecola following the large earth flow that occurred in February 1961 (**Figure 1-6**). This deep-seated landslide at Ecola Point (here termed the Ecola Point Landslide) damaged 125 acres and caused severe damage to the park, which resulted in its closure for 10 months. During the initial movement of the landslide in 1961, the slide was moving at approximately 3 ft/day. Later the landslide slowed down and then stopped two weeks after it began moving. North and Byrne (1965) noted that the slide was constrained between two basalt masses at the shoreline. Sediments deposited along its toe had been greatly eroded by ocean waves by 1965. North and Byrne (1965) observed that the slide began as a debris slump, exhibited a vertical displacement of 40 ft at the crown and a maximum horizontal displacement of 100 ft at the middle. Schlicker and others (1961) also mapped landslide activity on the Ecola Park Road Landslide (just south of the current park entrance booth) as well as a portion of the Bald

Point Landslide just south of Indian Beach (**Figure 1-6**). North and Byrne (1965) observed that erosion by wave action had removed material from the toe of the Bald Point Landslide, leaving only basalt boulders and cobbles to outline its extent. They suggested that the basalt base may protect Bald Point from complete erosion by waves.

Carson and Hankel (1975) described several landslide movements at Ecola that occurred late in the winter of 1975. For example, ~4,900 yd^3 of material flowed down the cliff at Crescent Beach in January 1975, and by the end of the month, most of the landslide sediment had been removed by waves. This slide is probably the Ecola Park Road Landslide located at the north end of Crescent Beach (Plate 2). In addition, the Ecola Point Landslide that had moved so spectacularly in 1961 began moving again over a two-week period in late January and early February 1975, resulting in closure of the park for four months. Carson and Hankel (1975) observed that the period of landsliding had coincided with months of high rainfall.

In December 2016, Pfeiffer provided observations and mitigation recommendations for the Indian Beach Road Landslide (here termed the Canyon Creek Landslide) and the Ecola Access Road Landslide (Ecola Park Road Landslide). Pfeiffer described the Canyon Creek Landslide as ~250-ft wide and ~300-ft long with a 2-ft vertical displacement in the road. This landslide extends ~300 ft downslope to Canyon Creek (**Figure 1-7**). Most recently, Wavra (2021) described the Canyon Creek Landslide and provided recommendations for mitigation.

Pfeiffer (2016) estimated the Ecola Park Road Landslide to be 700 ft wide, with the northern extent of sliding occurring just 400 ft south of the entrance booth to the park. The slide surface was observed near the top of the very steep cliff down to Crescent Beach, approximately 350 ft downslope from the road (**Figure 1-7**).

Figure 1-6. Landslide map of the southwest portion of Ecola from Schlicker and others (1961).

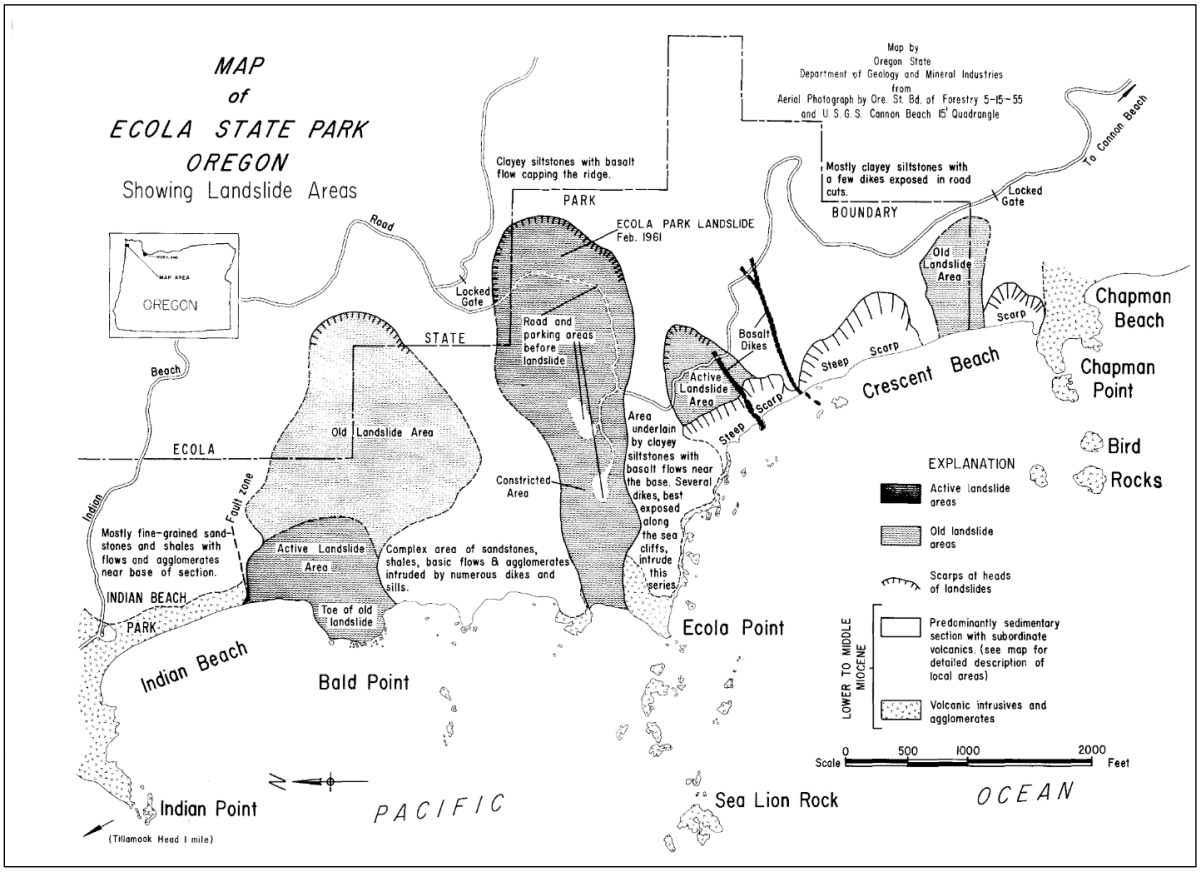

Figure 1-7. Maps of the Canyon Creek Landslide (left) and Ecola Park Road Landslide (right) from Pfeiffer (2016).

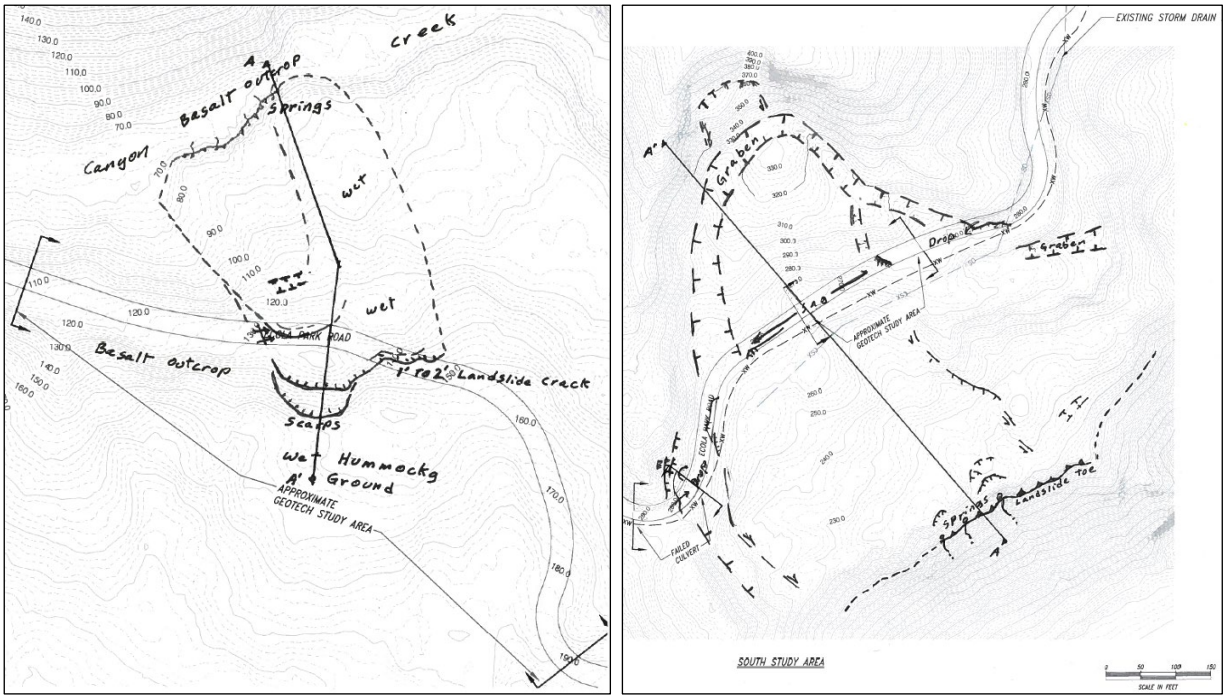

In February 2020, the Ecola Park Road Landslide reactivated, damaging the main entrance road and closing the park again. A section of trail as well as several trees and salal bushes were sent cascading over the cliff edge, confirming Schlicker and others (1961) and Pfeiffer (2016), both of which mapped the landslide toe by the cliff edge.

In 2021, Burns and others published a lidar-based landslide inventory of coastal Clatsop County, including all of Ecola (**Figure 1-8**). To create the detailed landslide inventory, two tasks were performed. First, landslide deposits were identified and characterized using lidar-derived topography and supporting GIS datasets such as the underlying geology and slope. This was followed by several days in the field to inspect key deposits. The methodology for these tasks is described in detail in DOGAMI SP-42 (Burns and Madin, 2009). Burns and others (2021) mapped 270 mass movement areas within the Ecola study area. 91 of those are within Ecola, 90 are within Elmer Feldenheimer State Natural Area, and the rest are in the surrounding private property. Although many landslides have occurred in the study area (**Figure 1-8**), the landslide mapping method delineates areas where landslides have not occurred.

In 2000, Wiley created a map of western Oregon with estimates of 24-hour rainfall intensity that could potentially initiate debris flows (**Figure 1-9**). These types of landslides are generally shallow, but can move rapidly down slope and, in some cases, when channelized, can grow as they travel down slope. At Ecola, Wiley (2000) estimated that 5 in–6 in of rain in 24 hours would likely trigger shallow rapid landslides (i.e., debris flows). As shown in **Figure 1-2**, Ecola can experience as much as 160 in of rain in a winter season. Individual storms can deliver as much as 5 in–10 in in a 24-hour period (Wiley, 2000). We provide these numbers as guidance to OPRD so they can monitor rainfall and be more aware of conditions in which shallow landslides might be more likely.

Figure 1-8. Landslide mapping of Burns and others (2021) in Ecola following DOGAMI SP-42 method (Burns and Madin, 2009).

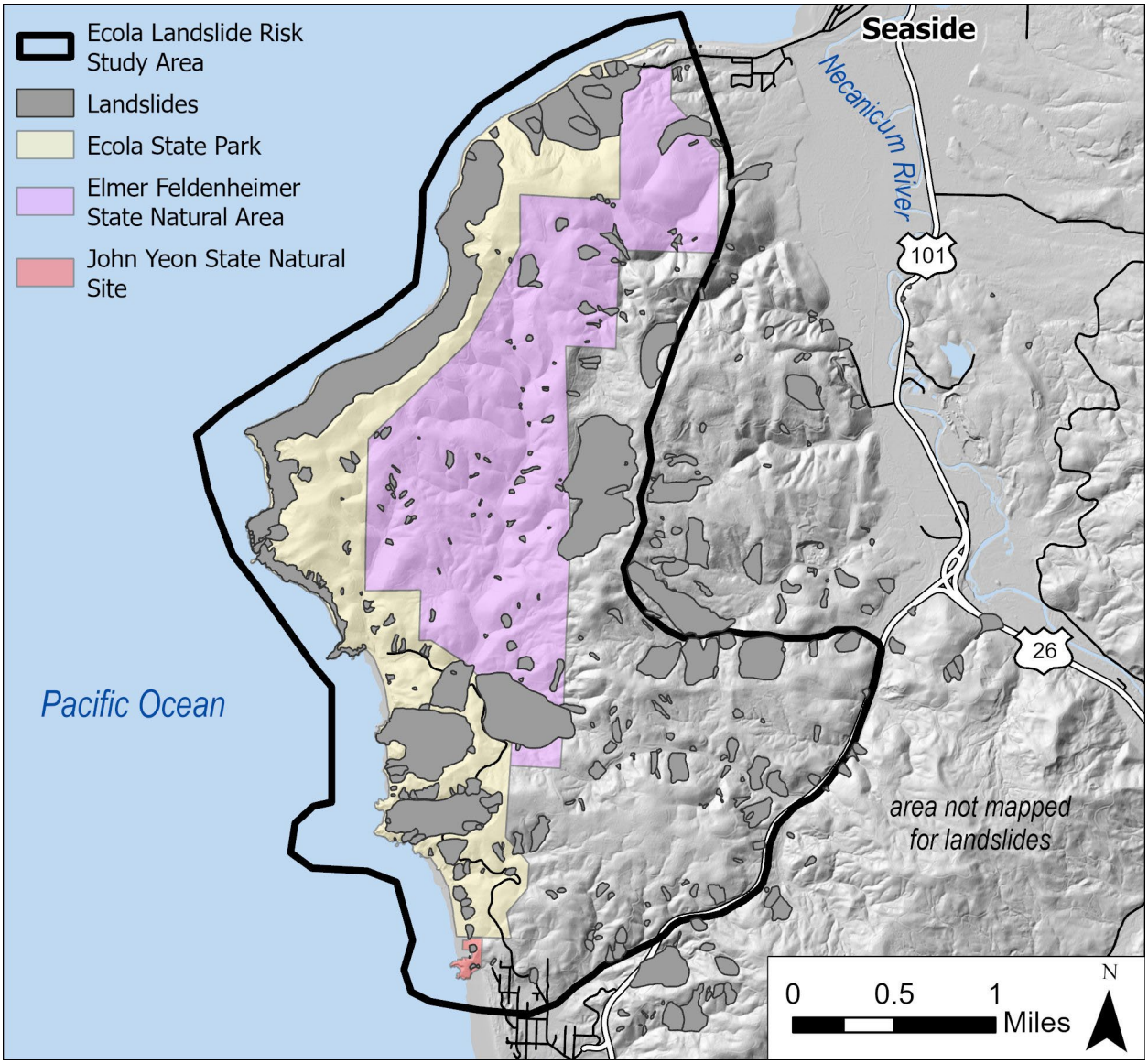

Figure 1-9. Map of estimated 24-hr rainfall that would likely trigger debris flows (Wiley, 2000). Ecola region is outlined in the black box on map.

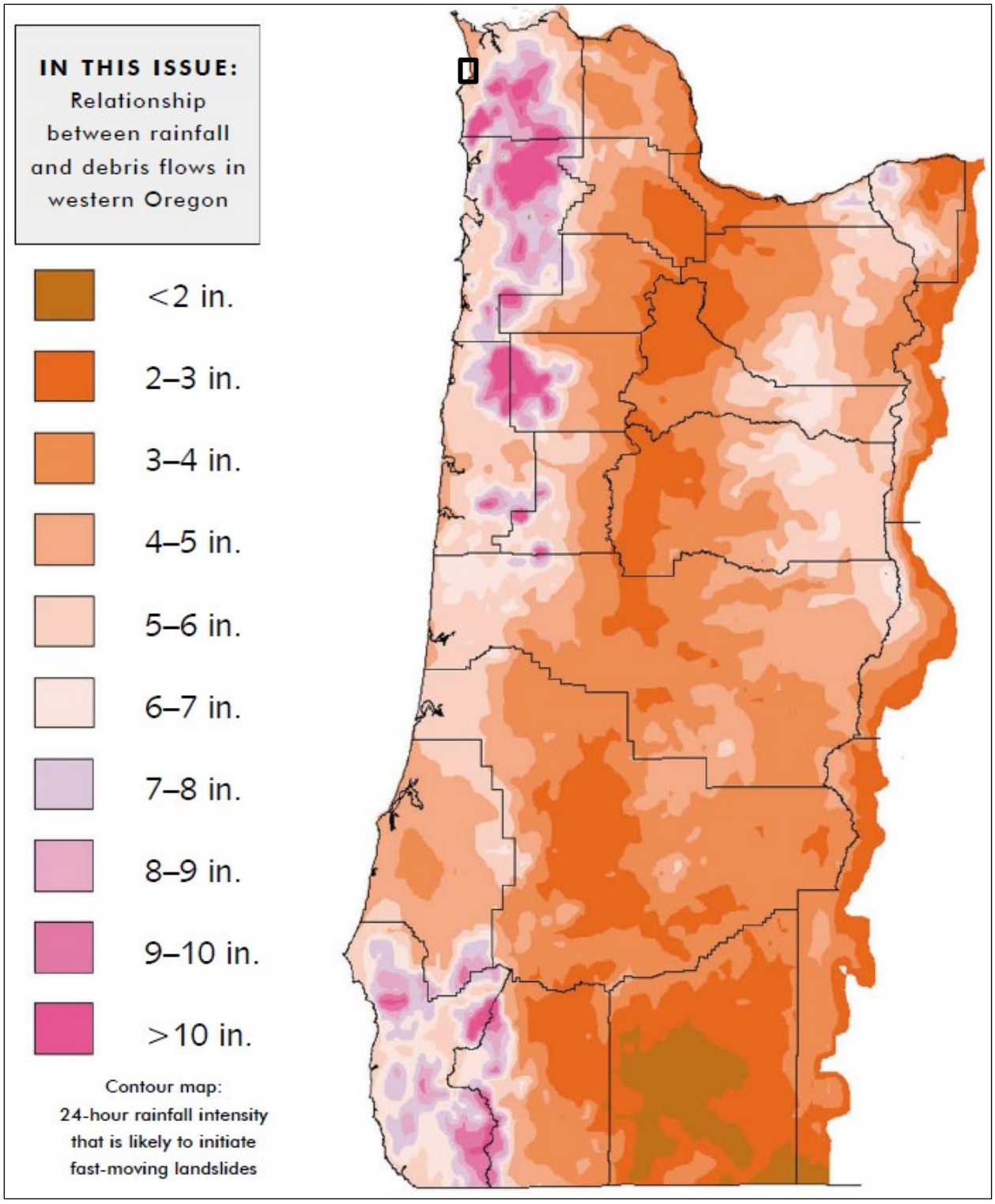

2.0 METHODS

This section describes the methods followed to produce the landslide risk map and the recommendations for landslide risk reduction. The first task was the collection of a new airborne lidar within the study area, from which bare-earth models of the ground surface could be analyzed. This latest lidar dataset has enabled us to perform change mapping between the new (2023) lidar topography and the previous lidar data collected in 2009. The second task was to perform landslide risk analysis, including creation of a landslide risk map with recommendations for future risk reduction. Several datasets were created and used to perform the landslide risk analysis and create a landslide risk map. The methods we followed to create these datasets are described below.

2.1 Lidar Datasets

In this study, two lidar point-cloud datasets were used to develop a vertical difference raster to help quantify the movement of landslides over a recent 14-year period (2009-2023) in Ecola. Both datasets were collected under the management of the Oregon Lidar Consortium (OLC) at DOGAMI. The lidar for both datasets were acquired by the same Oregon-based remote sensing firm, NV5 Geospatial, which was previously known as Watershed Sciences at the time of the North Coast 2009 acquisition. The first lidar dataset used is the DOGAMI OLC North Coast 2009 Lidar Project, and the second lidar dataset used is the DOGAMI OLC Ecola State Park 2023 Lidar project, collected as part of this project. For the lidar data from both collections, NV5 Geospatial/Watershed Sciences utilized automated and manual processes to compute the lidar data and make the specified project deliverables. These include GPS control calculations, trajectory calculations, kinematic corrections, sensor and data calibration, and lidar point classification.

For both projects, upon delivery from the vendor, DOGAMI staff independently reviewed all lidar data and associated deliverables and checked for completeness and data quality, which includes examining the lidar data for errors associated with internal data consistency, model quality, and accuracy. Visual checks of the datasets were also carried out to identify potential data artifacts and misclassifications. For any errors found, the vendor used both manual and automated methods to reclassify or remove points, and then a second round of quality control analysis was performed by DOGAMI to ensure that all known errors were corrected, so that the final data is free of misclassifications and topographic processing artifacts. The accuracy of each lidar project was determined by comparing lidar elevation of the classified surface/ground points with GNSS survey control points to quantify absolute vertical and horizontal accuracies. Delivery items for each dataset included bare-earth/DEM rasters, highest hit/DSM rasters, intensity rasters, a.las point cloud with classified ground (Version 1.1 for the 2009 dataset and Version 1.4 for the 2023 dataset), real-time kinematic (RTK) and survey checkpoint datasets with associated geodetic monuments, vector files for the project (including tiling schemes, project areas, and flightline data), and a comprehensive data report detailing data acquisition, collection methods, data processing, and data validation information. During data collection, it is common for some types of land surfaces, such as dense vegetation, to return fewer pulses to the sensor, which will cause variation in the point density throughout the project area due to terrain, land/vegetation cover, and water bodies. This results in higher spatial resolution in some areas of the project area and lower resolution in other areas, however, all areas within the projects met the standard DOGAMI OLC accuracy requirements at time of acquisition.

The prechange/control dataset used in this study is the DOGAMI OLC North Coast 2009 Lidar Project and was collected with methods and spatial references that differ somewhat from current Oregon Lidar

Consortium practices. We needed to first select the overlapping portion of the 2009 dataset and make the data format and coordinate system compatible with the 2023 data. The North Coast 2009 lidar project was divided into 11 separate deliveries that were collected over multiple months. The lidar data used for this study is from the North Coast Delivery 1 segment, which was collected between 04/05/2009 and 05/10/2009, over a total area of approximately 97,176 acres/152 mi^2. This study utilized the 6,158 acres/9.6 mi^2 portion of the data that fell within the current study area. For the 2009 collection, the lidar data was delivered in the NAD 1983 (HARN) horizontal datum using Oregon Statewide Lambert projection with international feet units, utilizing the NAVD88 (Geoid03) vertical datum (Watershed Sciences, 2009). The specific lidar sensor used for this collection was not recorded in the associated project data report. Based on the RTK GPS survey point comparison to the nearest laser point, the absolute vertical accuracy of this collection was 0.10 ft (RMSE), and the average pulse density per square meter (ppsm), as calculated from first returns, was 7.33 ppsm (Watershed Sciences, 2009). Ground point density for the entire Delivery 1 of the North Coast 2009 project was 0.15 point/ft^2. However, as in all lidar data, this density varies according to the terrain, vegetation cover, and water bodies within the survey area.

The DOGAMI OLC 2023 Ecola Lidar project is the most recent dataset used to quantify vertical change in topography for the Ecola area. This lidar dataset was contracted for this specific project and designed to achieve a highly accurate ground model. The entire 2023 dataset was acquired on March 17, 2023, and the of 6,158 acres/9.6 mi^2 project area encompassed the entire Ecola, Elmer Feldenheimer State Natural Area, and adjacent areas west of Highway 101 between Seaside and Cannon Beach. The lidar collection was accomplished by using a Reigl VQ-1560ii-S lidar sensor, mounted in a Cessna Grand Caravan aircraft. The sensor can record unlimited returns per pulse, and up to 15 returns per pulse can be delivered in the current LAS 1.4 file format. The project was planned to achieve an average of at least 20 ppsm (NV5 Geospatial, 2023). The lidar data and all associated deliverables were generated using the NAD83(2011) horizontal datum in the Oregon Statewide Lambert projection, with units in international feet, and utilized the NAVD88 (Geoid18) vertical datum (NV5 Geospatial, 2023). Bare-earth DEMs were gridded at 3-ft resolution. Although this resolution is equivalent to the 2009 data, the grid cells of the two datasets are offset by a half grid cell (1.5 ft), due to a change in convention for OLC lidar products.

All portions of the project area were collected with 100% overlap, which equates to 50% sidelap per flightline. This double-coverage collection method resulted in pulses from different incident azimuths for all portions of the project area, creating a dense lidar point cloud that has greater penetration in areas of dense vegetation or tree cover. The average lidar point density is approximately 2.87 points/ft^2, with an average of 0.40 points/ft^2 for ground classified points in the project area (NV5 Geospatial, 2023). The dense ground classified points (2.7 greater density than the 2009 data) are essential for creating a more accurate change detection product. The absolute vertical accuracy of the lidar data for the whole project area averaged to around 0.0196 ft when compared to the lidar point cloud and averaged to around 0.0164 ft when compared to the bare-earth DEM. In highly vegetated areas with dense tree cover, the vertical accuracy averaged to 0.0820 ft when compared to the lidar point cloud (NV5 Geospatial, 2023). The vertical accuracy in vegetated areas of the 2023 data was similar to or better than the absolute accuracy of the 2009 data collected on unvegetated surfaces.

To complete a change detection analysis, DOGAMI staff compared the point clouds of the 2009 and 2023 data and then subtracted the 2009 data from the 2023 data to distinguish areas of vertical topographic change. First, the 2009 data had to be transformed reprojected into the same datum and projection as the 2023 data. This was accomplished by loading the 2009 NAD83(HARN) point cloud into a CAD program and using the Terrasolid suite of software tools to transform the point cloud into NAD83(2011), to be coincident with the 2023 data. The vertical datums of the two datasets are both

versions of the NAVD88 datum. A check of the difference between the realizations of the NAVD88 vertical datum using the Geoid03 and Geoid18 models using the NOAA VDatum v. 4.6.1 program (https://vdatum.noaa.gov/welcome.html) showed a vertical difference of ~0.2 ft–0.3 ft over the study area, with lower elevations in the more recent version of the datum. Due to software limitations and the relatively small offset between the two geoids, we did not transform the vertical coordinates of the 2009 data to Geoid18. Preliminary differencing of the two datasets in the same horizontal coordinate system showed systematic vertical differences across ridgelines and over apparently stable landscape features exceeding 1 ft. These discrepancies indicated vertical and horizontal mismatches greater in magnitude than what can be explained by differences in datums. The systematic shift likely results from less accurate Global Navigation Satellite System and lidar collection technology as well as flight design, ground control, and processing strategies used during the 2009 data collection.

To fix the observed offset over stable areas, DOGAMI staff loaded both point clouds into QT Modeler geospatial software, and manually adjusted the X, Y, and Z position of the 2009 data over distinctive point and line features and areas of minimal vertical relief to minimize both vertical and horizontal mismatch between the 2009 and 2023 point clouds. The shift accounted for the average vertical difference between geoid models as well as the larger survey discrepancy between lidar datasets. The 2009 data were manually adjusted by +3.6 ft in grid easting, -2.0 ft in the grid northing, and +1.4 ft in the up direction. After applying the 3-D shift to the 2009 data, both point clouds were then regridded and a new bare-earth/DEM surface was created in ArcGIS for both datasets using the same tools and input parameters for each project. Next, the 2009 data were clipped out of the original delivery extent to precisely match the extent of the 2023 project collection area. DOGAMI then utilized the raster calculator in ArcGIS to subtract the 2009 bare-earth DEM from the 2023 bare-earth DEM to create an overall change raster for Ecola. The root mean square (RMS) error of the entire difference raster is ±2.5 ft (**Table 2-1**). This statistic includes both residual systematic discrepancies and local large-magnitude change over areas of landsliding and coastal change. When the areas of natural change recognized in this study are excluded, the RMS error difference between datasets is ±1.7 ft (**Table 2-1**) and the mean value for the offset between the two datasets is 0.33 ft. We attribute this error mainly to the age and collection parameters of the two datasets, with the calibration and alignment of the 2009 dataset being much less robust than the advanced and highly accurate 2023 lidar dataset. In addition to geometric errors in the 2009 data, the lower ground return density in the 2009 data and differences in the ground classification between datasets produces apparent vertical discrepancies between the two. The ~2-ft RMS difference provides a general measure of the level of change that can be recognized in the difference raster with confidence.

Table 2-1. Calculated RMS difference between the 2009 and 2023 lidar datasets

Type of Change Raster	RMS vertical difference between 2009 and 2023 datasets
Change raster of entire project area	+/-2.5 ft
Change raster of project area, excluding areas of known landslide movement	+/-1.66 ft

2.2 Geology Update

An updated onshore digital geologic map was created for Ecola in GIS through heads-up digitizing of an unpublished 1:24,000-scale paper geologic map provided by Niem and others (unpublished data, 2024)(Plate 2). The map was rectified to a lidar base map and converted into a digital format consistent with the USGS National Cooperative Geologic Mapping Program Schema (GeMS; USGS NCGMP, 2020). Additional polygons of Quaternary surficial units were mapped along beaches following Witter and others (2009), and alluvium was mapped along the major streams based on lidar inspection and field checking. Plate 2 displays the geologic data at a scale of 1:8,000.

2.3 Lidar Change Mapping

The two lidar bare-earth DEM datasets (2009 and 2023, 14 years) were differenced (2009 subtracted from 2023) in GIS, which results in a change dataset. The change dataset has values of change throughout most of the study area. From field observations, we know that the large percentage of apparent elevation changes was error between the two datasets within the area. So, we implemented the use of a cutoff (threshold) value for removing noise within the change dataset to increase our ability to locate probable landslides, as recommended by Burns and others (2010) and Burns and others (in press). Two threshold values were used during the mapping, depending on the scale of mapping: 1) approximate RMSD of change datasets ±2 ft; and 2) no threshold.

We followed the general methods developed by Burns and others (in press). Mapping was performed at a range of scales from 1:10,000 to 1:2,000. All mapped landslide GIS data were finalized at 1:2,000. All mapping was performed using GIS software with the following primary datasets:

- Before-and-after DEMs converted to hill shades and slope shades
- Before-and-after 3-ft elevation contours
- Lidar-based change datasets with various thresholds
- Aerial photos

Thresholds of change were applied to the change datasets to aid in visualizing the data at various spatial scales. In general, higher thresholds were used at smaller scales and lower thresholds at larger scales. We attributed four fields for each polygon during mapping:

- Primary process
- Event unique id
- Difference dates
- Notes

The primary process field was attributed with one of the following predetermined choices (DF=debris flow):

- DF Initiation – In-channel initiation (erosion)
- DF Initiation - Roadfill embankment (erosion)
- DF Initiation - Road cut slope (erosion)
- DF Initiation - Deep landslide (evacuated)
- DF Initiation - Shallow landslide (evacuated)
- DF Transport - Predominantly erosion
- DF Transport - Predominantly deposition
- DF Transport - Predominantly transport (mixed erosion and deposition)
- DF Transport - Predominantly transport (no increase or decrease in volume)

- DF Deposition – Predominantly deposition
- Fall/topple (evacuated)
- Fall/topple (deposition)
- Deep landslide (evacuated)
- Deep landslide (deposition)
- Shallow landslide (evacuated)
- Shallow landslide (deposition)

Note that a single event may have numerous polygons, each with a unique ID, representing different primary processes. For example, a single debris flow event could have three polygons, including DF initiation, DF transport, and DF deposition. This allowed us to summarize observations at an event level. Finally, a field called "notes" was filled in with any additional information.

2.4 Serial Orthophoto Mapping

The lidar change analysis is accurate spatially, but it is limited to only 14 years (2009 to 2023). Orthophoto-based landslide inventory mapping is less accurate spatially but can provide data over a longer timeframe (Burns, 2007). We used historic serial orthophotos to create an additional landslide inventory dataset that spans the period from 1939 to 2022 (U.S. Department of Agriculture). The following orthophotos were used from the following datasets:

- 1939 - Southwest portion of the study area only
- 1967 - Entire coastal strip of the study area only
- 1975 - Southwest portion of the study area only
- 1995 - Entire study area (NAIP)
- 2000 - Entire study area (NAIP)
- 2005 - Entire study area (NAIP)
- 2009 - Entire study area (NAIP)
- 2011 - Entire study area (NAIP)
- 2012 - Entire study area (NAIP)
- 2014 - Entire study area (NAIP)
- 2016 - Entire study area (NAIP)
- 2018 - Entire study area (NAIP)
- 2020 - Entire study area (NAIP)
- 2022 - Entire study area (NAIP)

U.S. Army Corps of Engineers, 1939, 1967, 1975: Aerial photographs of the Oregon Coast.
U.S. Department of Agriculture, NAIP Digital Ortho Photo Images. Oregon Statewide Imagery Program (OSIP), geohub.oregon.gov/datasets

We estimate the total timeframe of landslide inventory captured by this analysis to be approximately 83 years (~1939 to 2022). After each landslide was mapped, two fields, landslide type and date range, were attributed for each polygon.

2.5 Field Data Collection

We spent approximately one week driving and walking Ecola roads and trails, mapping features of landslide movement. We also spent time checking the geology and results from orthophoto and lidar change mapping. Field data were used to edit landslide and geology datasets.

2.6 Landslide Susceptibility and Risk

To make the landslide susceptibility and risk dataset, we combined several datasets and selected appropriate portions of published landslide susceptibility methods. The two methods we used portions of are Burns and Mickelson (2016) and Burns and others (2012). We used the retrogression zones from Burns and Mickelson (2016) to identify susceptible regions upslope of deep landslide head scarps. Most deep landslides tend to have a steep head scarp above the failed mass. The head scarp area will commonly fail retrogressively, or, a separate landslide will form above the head scarp because of the loss of resisting forces directly adjacent to and below the head scarp. To account for the increase in susceptibility of the area above head scarp, we applied a buffer around the head scarp-flank polygons (Burns and Mickelson, 2016). We also used a portion of the shallow landslide stability calculation resulting in a factor of safety (FOS) from Burns and others (2012).

The following datasets and methods were combined to create a landslide susceptibility map of the study area:

- SP-42 lidar-based landslide inventory
- Protocol for deep landslide susceptibility mapping, Special Paper 48, retrogression zone
- Serial orthophoto landslide inventory (1939–2022)
- Protocol for shallow-landslide susceptibility mapping, Special Paper 45, shallow landslide FOS susceptibility zones based on geologic units
- Serial lidar change analysis landslide inventory (2009–2023)
- Field-based data collection and previous landslide studies

The combined datasets were processed, analyzed and classified into one of the following landslide susceptibility zones:

- *None to Low*
- *Low*
- *Moderate*
- *Moderate to High*
- *High*
- *Very High*
- *Active*

Deposit and scarp-flank polygons created following the SP-42 mapping approach (Burns and others, 2021) were directly incorporated into the susceptibility map. The polygons were classified as *Moderate to High* if characterized as prehistoric and *High* if characterized as historic. Regions within the study area with no mapped landslide deposit were classified as *None to Low* for this layer of the final risk map.

Most landslides tend to have a steep head scarp above the landslide body. The head scarp area will commonly fail retrogressively, or a separate landslide will form above the head scarp because of the loss of resisting forces directly adjacent to and below the head scarp. To account for the increase in susceptibility of the area above head scarp, we apply a buffer around the scarp-flank polygons following the method outlined in Burns and Mickelson (2016). We classified the buffer zones as *None to Low* (no

landslide), *Low* if mapped as prehistoric, and *Moderate* if mapped as historic. The size of the buffer was also dependent on the relative age of the landslide. If classified as prehistoric, a 1:1 horizontal to vertical distance (1H:1V) buffer was applied and if classified as historic, a 2H:1V buffer was applied.

Landslide polygons from the serial orthophoto landslide inventory were also directly incorporated into the susceptibility map. The polygons were classified as *Very High*, which indicates the landslide had moved more than once in the last ~150 years.

When delineating shallow landslide hazard zones, one of the main factors is steepness of slope. Different geologic units have different material properties, and thus, will have different slopes susceptible to future shallow landslides. To identify areas more susceptible to future shallow landslides, the method calculates the slope stability FOS. A FOS >1.0 theoretically represents a stable slope because the shear resistance (or strength) is greater than the shear stress. A FOS <1.0 theoretically represents an unstable slope because the stress is greater than the shear strength. A critically stable slope has a FOS = 1.0. Because it is impossible to know all the conditions present within a slope, most geotechnical engineers and engineering geologists recommend that slopes with a FOS <1.5 be considered potentially unstable (Turner and Schuster, 1996; Cornforth, 2005). The approach of Burns and others (2012) is intended to delineate shallow landslide susceptibility for a large region, for example a county. Because the area in this study is much smaller than the intended use of SP-45, we modified the procedure and classified slopes within the geologic units as *None to Low* if the FOS is greater than 1.25, and *Moderate* if the FOS is less than 1.25. We used the strength and resulting slope angles developed in the Landslide Hazard and Risk Study of Tillamook County, Open-File Report O-20-13, (Calhoun and Burns, 2020).

As a result of the recent lidar acquisition (2023), we consider the landslide polygons mapped using the lidar change dataset (2009–2023) to have all moved relatively recently (~<20 years) or to be currently moving. Therefore, we classified all these polygons as *Active*.

The final datasets incorporated into the landslide susceptibility map were the data collected in the field and previously mapped landslides by Pfeiffer (2016). Because all these data are of landslides that have moved relatively recently (~<20 years) or are currently moving (2016–2024) we classified all these polygons as *Active*.

Table 2-2 displays a summary of all the datasets used to create the landslide susceptibility/risk zones and the relationships.

Landslide susceptibility zones from each input dataset were combined, with the precedence going to the higher susceptibility zone, into a single, contiguous GIS layer, which classifies every portion of the study area into one of the seven zones. The zones were defined and estimates of landslide-recurrence movement rates established. Additionally, recommendations for future development were added to each of the zones. The addition of the recommendations and the park infrastructure on Plate 6 adds the risk component to the susceptibility.

Table 2-2. Landslide susceptibility/risk matrix detailing input datasets with relevant attributes and relative levels of risk.

Dataset	Area (polygons or zones)	Attribute	Susceptibility/Risk Zone
SP-42 landslide inventory	-	Not a mapped landslide	*None to Low*
SP-42 landslide inventory	Deposits and scarp flanks	Prehistoric	*Moderate to High*
SP-42 landslide inventory	Deposits and scarp flanks	Historic	*High*
SP-42 landslide inventory	Scarp flanks	Prehistoric 1H:1V buffer	*Low*
SP-42 landslide inventory	Scarp flanks	Historic 2H:1V horizontal	*Moderate*
Aerial photo landslide Inventory	-	Not a mapped landslide	*None to Low*
Aerial photo landslide Inventory	Deposits and scarp flanks	Landslide moved at least once in the last ~100 years	*High*
Aerial photo landslide Inventory	Deposits and scarp flanks	Landslide moved more than once in the last ~100 years	*Very High*
Landslide susceptible geologic units	Geologic units	No mapped landslides within the unit	*None to Low*
Landslide susceptible geologic units	Geologic units	Unit has some overlapping landslides (~7–17%)	*Low*
Landslide susceptible geologic units	Geologic units	Unit has many overlapping landslides (~>17%)	*Moderate*
Shallow landslide susceptible areas	Geologic units and slope map	FOS >1.5	*None to Low*
Shallow landslide susceptible areas	Geologic units and slope map	FOS = 1.5–1.25	*Moderate*
Shallow landslide susceptible areas	Geologic units and slope map	FOS <1.25	*Moderate to High*
Serial lidar landslide inventory	-	Not a mapped landslide	*None to Low*
Serial lidar landslide inventory	Mapped landslide	Very recently or currently moving/active	*Active*
Field data and previously mapped landslide studies	-	Not a mapped landslide	*Low to none*
Field data and previously mapped landslide studies	Mapped landslide	Very recently or currently moving/active	*Active*

3.0 RESULTS

Our lidar-based landslide inventory resulted in the identification of 270 discrete mass movements that have likely occurred in the study area at some point in the past (Plate 3). Of these, 91 are inside Ecola. About 50% were characterized as having moved within the last 150 years (historic), the other half demonstrated subdued features leading to their characterization as having moved more than 150 years ago (prehistoric).

The results of the 87-year serial orthophoto mapping are displayed on Plate 4 and summarized in **Table 3-1**. We identified a total of 72 landslides that moved between 1939 and 2022. If annualized, this dataset suggests that there is approximately one landslide per year within the study area. Many of these historic landslides coincide with deposits from the SP-42 lidar-based landslide inventory. There was almost complete agreement in landslide age as well, with the coinciding inventory deposits all classified as historic.

Table 3-1. Summary of the serial orthophoto landslide mapping. Note the two highest percentages of the total are timeframes with extreme storm events: December 1964 and February 1996.

Aerial Photo Timeframe	Number of Landslides Mapped During this Study in the Timeframe	Percent of Total Mapped Serial Orthophoto Landslides
Pre-1939	3	4%
1939–1967 Extreme storm Dec 1964	15	21%
1967–1975	0	0%
1975–1995	14	19%
1995–2000 Extreme storm Feb 1996	17	24%
2000–2005	4	6%
2005–2009	2	3%
2009–2011	1	1%
2011–2012	0	0%
2012–2014	5	7%
2014–2016	0	0%
2016–2018	0	0%
2018–2020	3	4%
2020–2022	11	15%
Total	**72**	**100%**

The results of the 14-year serial lidar mapping are displayed on Plate 5 and summarized in **Table 3-2.** The 2009 and 2023 lidar DEMs were differenced (the newer topographic elevation dataset was subtracted from the older, revealing areas of topographic change) and areas of movement were mapped using the change dataset. 100 discrete areas considered to represent landslide activity were mapped. Approximately 40% were characterized as shallow, 50% as deep, and 10% as debris flows. If annualized, this dataset suggests that there are approximately seven landslides per year within the study area. Again, many of the landslides coincide with deposits from the SP-42 lidar-based landslide inventory. There was almost complete agreement in landslide age as well, with the coinciding inventory deposits all classified as historic.

Table 3-2. Summary of serial lidar landslide mapping. Because some of the landslides overlap spatially, the total count is more than the 100 total areas of movement.

Primary	Count
Deep landslides	19
DF Initiations – In-channel initiation	2
DF Initiations - Shallow landslide	8
Falls/topples	2
Fill settlements	5
Shallow landslides	84

The final landslide susceptibility and risk map is displayed on Plate 6, while **Table 3-3** provides definitions of each level of susceptibility and risk (derived from **Table 2-2**) along with an estimate of when future landslide activity may occur and recommendations for future development.

Table 3-3. Landslide susceptibility and risk matrix. CEG stands for a certified engineering geologist which is a license required to practice in Oregon. PE stands for a professional engineer which is a license required to practice in Oregon. For landslide evaluation and mitigation design a Geotechnical Engineering (GE) is recommended.

Landslide Susceptibility and Risk Zones	Zone Definition	Recurrence Estimate	Recommendations
None to Very Low	No mapped landslides and has little or no factors related to future landslides.	NA	Acceptable to develop under general direction from a CEG or PE.
Low	No mapped landslides but has some landslide factors, including: 2:1 scarp/flank buffer (prehistoric).	NA	Acceptable to develop under general direction from a CEG or PE.
Moderate	No mapped landslides but has some landslide factors, including: 1:1 scarp/flank buffer (historic) and/or shallow FOS <1.25.	Greater than ~150 years	Acceptable to develop under direction from a CEG or PE. Detailed local slope stability analysis should be performed prior to development. Development should be done so that there is greater stability post development.
Moderate to High	Is a mapped landslide but has no evidence of movement in the last ~150 years.	Greater than ~150 years	Caution should be taken if considering development in these areas. Develop only under direction from a CEG or PE. Detailed local slope stability analysis should be performed, including proposed development prior to development. Development should be done so that post development ensures greater stability. Development in these areas is very likely going to require slope stabilization measures. Consider development with minimal infrastructure (e.g., trails) to reduce risk.
High	Is a mapped landslide and has evidence of movement at least once in the last ~150 years.	~50 to 150 years	Caution should be taken if considering development in these areas. Develop only under direction from a CEG or PE. Detailed local slope stability analysis should be performed, including proposed development prior to development. Development should be done so that post development ensures greater stability. Development in these areas is very likely going to require slope stabilization measures. Consider development with minimal infrastructure (e.g., trails) to reduce risk.
Very High	Is a mapped landslide and has evidence of movement more than once in the last ~100 years.	Less than ~50 years	Great caution should be taken if considering development in these areas. Develop only under direction from a CEG and PE. Detailed local slope stability analysis should be performed, including proposed development prior to development. Development should be done so that post development ensures greater stability. Development in these areas requires slope stabilization measures.
Active	Is a mapped landslide and has evidence of multiple movements in the last ~100 years or is currently active.	Active or less than ~50 years	Great caution should be taken if considering development in these areas. Develop only under direction from a CEG and PE. Detailed local slope stability analysis should be performed, including proposed development prior to development. Development should be done so that post development ensures greater stability. Development in these areas is going to require slope stabilization measures.

There are several notable landslides in Ecola (Plate 3) that are described, discussed, and summarized in detail below.

3.1 Ecola Park Road Landslide

The Ecola Park Road Landslide is an active deep rockslide-rotational landslide. The park's only entrance, along with utilities underneath the road surface, traverses the entire slide and has been routinely damaged throughout the years as a result. Our research shows this landslide was active in 1961, 1975, 2016, and 2024. In addition to these known movements, records of visitors recreating in the park indicate significant decreases in visitations in 2011, 2021, and 2022 that coincided with closure of the park due to slumping of the road and needed repairs (B. Cox, pers communication, October 2024). The failure surface appears to be perched approximately 185 ft above sea level (**Figure 3-1, Figure 3-2,** Plate 3). Therefore, the ocean waves are unlikely to reach this elevation and erode the toe. However, the lack of any horizontal land surface below this landslide (e.g., the beach) results in the calving of the toe material onto the cliff and beach below (yellow arrow 1 on **Figure 3-2**). This process results in the complete removal of the toe/resisting-force region of this landslide making it very susceptible to frequent future movements. The removal of the resisting-force region along the toe results in a transfer of loss of resisting forces to the middle portion of the landslide, inducing movement in the road area (yellow arrow 2 on **Figure 3-2**). This process continues to relocate up slope (or up the landslide body) in a metacronal wave (wavy movements produced by the sequential action as opposed to synchronized) similar to the way a centipede moves. The road movement transfers a loss of resisting force to the upper head scarp region inducing movement in this area below (yellow arrow 3 on **Figure 3-2**). The overall process was captured in the serial lidar change analysis (Plate 5). This process can also happen in the reverse order through the increase of driving forces at the head of the slide transferring to the middle and eventually the toe. This landslide is mapped as *Active* on the landslide susceptibility/risk map (Plate 6). Unfortunately, critical infrastructure (only public road in and out of the park and utilities) cross the central portion of this landslide and have been damaged repeatedly in the past and will likely continue to be damaged into the future unless this process is mitigated or avoided.

Figure 3-1. Ecola Park Road Landslide topographic map and cross section (A–B). Landslide features were mapped following the SP-42 method (Burns and Madin, 2009).

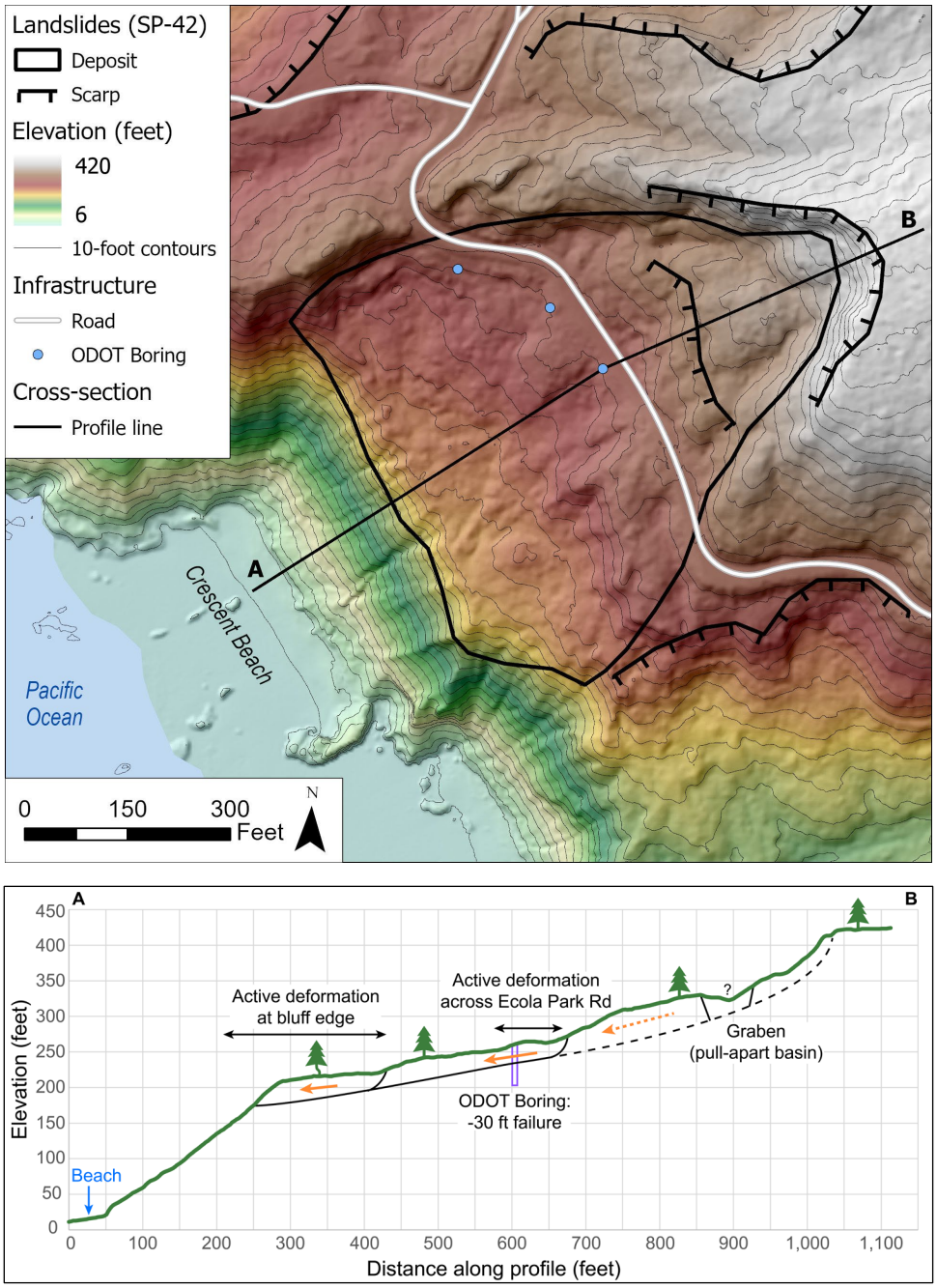

Figure 3-2. Serial lidar change map displayed in red and blue. Arrow #1 is in the area of toe movement and calving onto the beach cliff/beach below the approximate landslide failure surface. Arrow #2 is in the area of Ecola Park Road movement. Arrow #3 is in the area of head scarp retrogression.

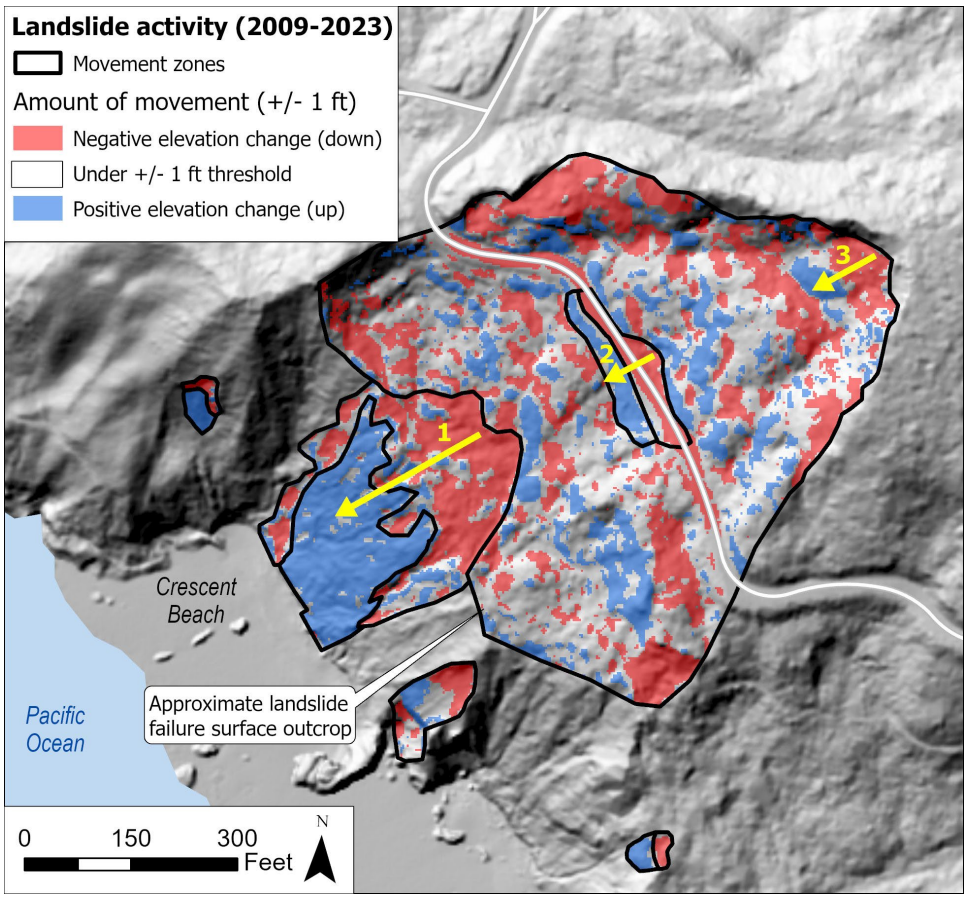

3.2 Cresent Beach Landslides

There are five smaller landslides along Cresent Beach in addition to the Ecola Park Road Landslide, all of which are considered to be *Active* or have likely moved in the past 150 years (Plate 3). Other than a hiking trail, no park infrastructure is on or near these slides. This group of landslides, all of which are characterized as a combination rockslide-rotational mass movement, appear to be directly influenced by the Pacific Ocean in the form of landslide toe erosion (**Figure 3-3**). As ocean waves slowly erode the toe of these landslides the resisting forces are reduced and will likely continue to result in episodic movement. This process was captured in the serial lidar analysis at the south end of Cresent Beach near Chapman Point (**Figure 3-3;** Plate 5).

Our aerial imagery analysis identified movement of all five slides at some point in the past ~100 years (Plate 4) and the serial lidar-based analysis captured a recent (since 2009) reactivation of the southernmost slide adjacent to Chapman Point (Plate 5). This is likely a lateral progression, meaning the landslide has become wider.

Figure 3-3. 2022 orthophoto showing recent landslide activity at two landslides along the southern end of Crescent Beach. Yellow lines delineate SP-42 landslide deposits and head scarps (Plate 3). Toe erosion has occurred on the slide at the north end of the image and reactivation has occurred adjacent to the southern slide. The reactivation is also captured in the serial lidar analysis (2009–2023; Plate 5).

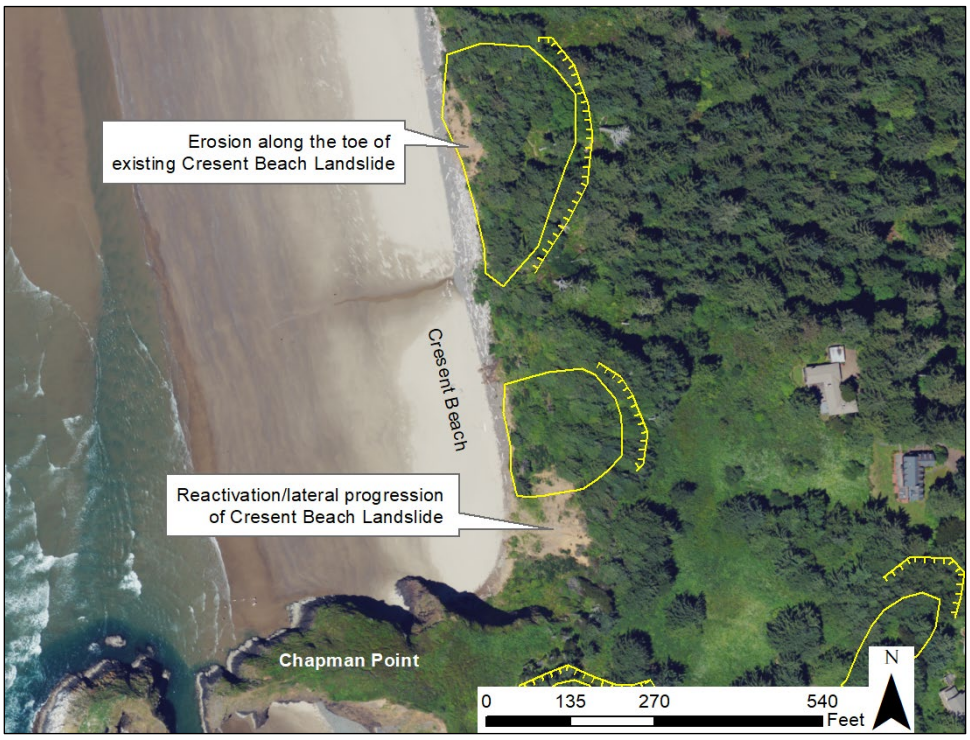

3.3 Ecola Point Landslide

The Ecola Point Landslide is mapped as a historic, deep, rockslide/rotational landslide and earth flow (**Figure 1-6; Figure 3-4**; Plate 3). This landslide is relatively flat (~10° slope) and the failure surface appears to be perched approximately 50 ft above sea level. This landslide's movement is most likely influenced by two main factors that increase pore-water pressure: 1) intense, prolonged precipitation and 2) rapid loading onto the landslide body. Earth flows generally mobilize during periods of prolonged intense rainfall. If the infiltration from the rain is faster than the soils can drain, increased pore-water pressure along the failure surface will result in movement (Keefer and Johnson, 1983). The other trigger is rapid loading onto the landslide body. The rapid loading in this case are shallow landslides along the flanks or the head scarp (yellow and teal arrows **Figure 3-4)**. The shallow landslide loads the Ecola Point Landslide rapidly, creating undrained conditions that result in increased pore-water pressures that allow earth flow to move on very shallow slopes (Keefer and Johnson, 1983). The overall process was captured in the serial orthophoto and serial lidar change analysis (Plate 4 and Plate 5**).** Both two main factors are present, making this landslide susceptible to future movements. Our research shows this landslide was active in 1961, which resulted in significant damage to park infrastructure, including roads, picnic areas, and parking lots (Schlicker and others, 1961). This landslide is mapped as *High* on the landslide susceptibility/risk map (Plate 6). Unfortunately, critical infrastructure (the only public road in and out of the park and utilities) cross the central portion of this landslide and have been damaged in the past; they will likely be damaged again in the future as the process reoccurs, unless this process is mitigated or avoided.

Figure 3-4. Map of the Ecola Point Landslide. The entire Ecola Point Landside moved and caused significant damage in 1961. Black arrow indicates overall direction of landslide movement. Yellow arrows indicate the direction of older, shallow landslides (rapid loading). Teal arrows indicate the direction of recent (2009–2023) landslides (rapid loading) onto the main landslide body. Landslide features were mapped following the SP-42 method (Burns and Madin, 2009).

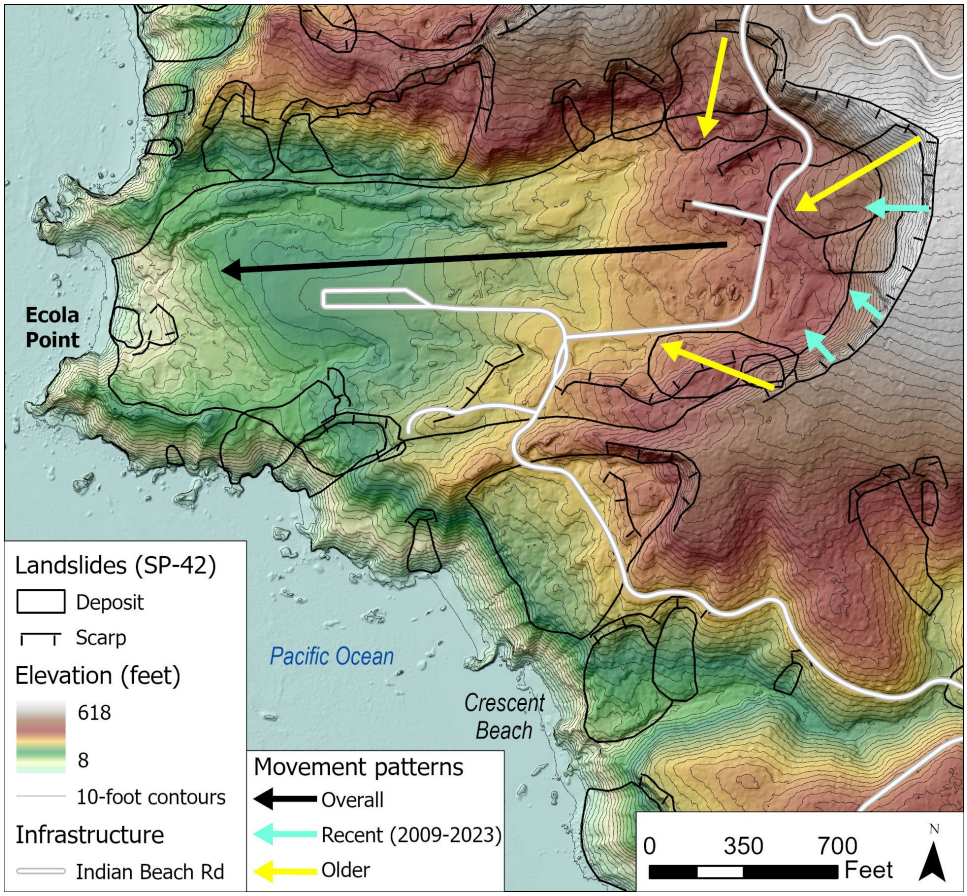

3.4 Bald Point Landslide

The Bald Point Landslide is also (e.g., Ecola Point Landslide) a historic, deep, rockslide/rotational landslide and earth flow (**Figure 1-6**; Plate 3). However, this landslide appears to be directly influenced by the Pacific Ocean in the form of landslide toe erosion (e.g., Cresent Beach Landslides) and is influenced by the two additional factors (intense precipitation and rapid loading) like the Ecola Point Landslide. The Bald Point Landslide experienced significant reactivation captured by the lidar change mapping (**Figure 3-5; Figure 3-6,** Plate 5). All three of these factors are present, making this landslide susceptible to future movements. Our research shows this landslide was active in 1939 and 2016 and shows signs of movement during the writing of this report in 2024. This landslide is mapped as *Active* on the landslide susceptibility/risk map (Plate 6). There is a hiking trail that traverses this landslide that was damaged in the 2016 movement, but fortunately, there is no primary infrastructure (roads, utilities, buildings) on or near this landslide.

Figure 3-5. Topographic map of the Bald Point Landslide (black outline). Landslide features were mapped following the SP-42 method (Burns and Madin, 2009).

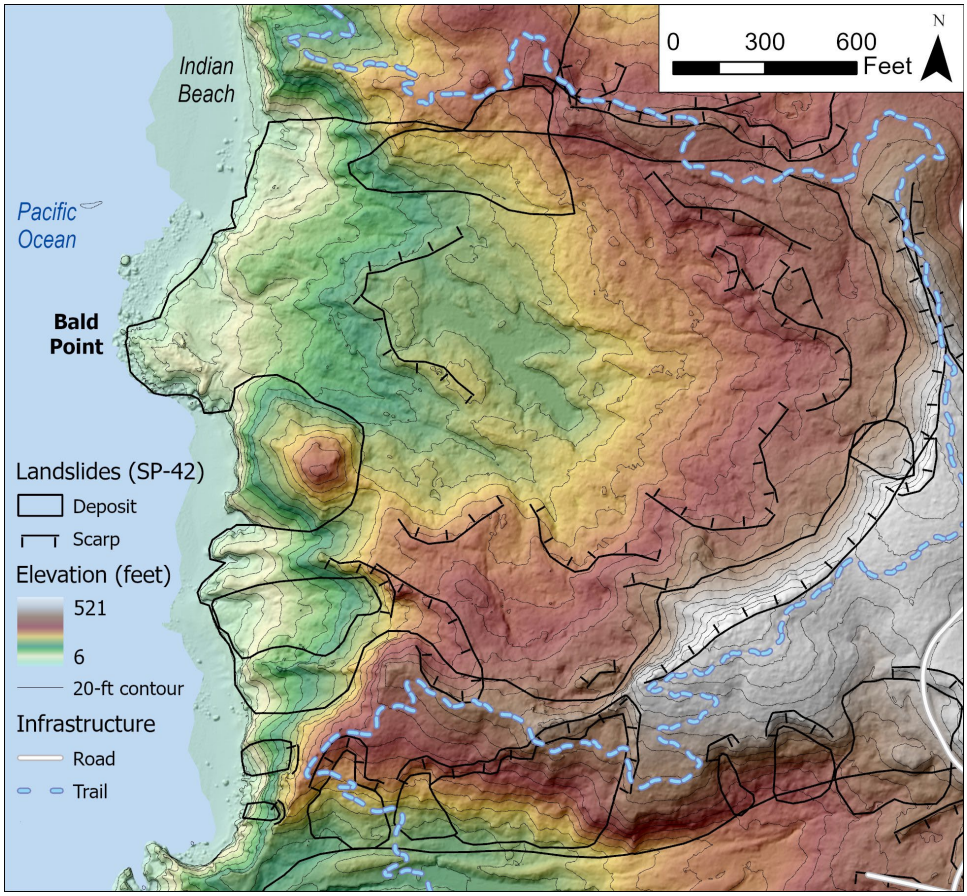

Figure 3-6. Serial lidar change map displayed in red and blue showing the significant reactivation captured by the serial lidar mapping (black outlines). Red indicates the ground moved up and blue indicates the ground moved down.

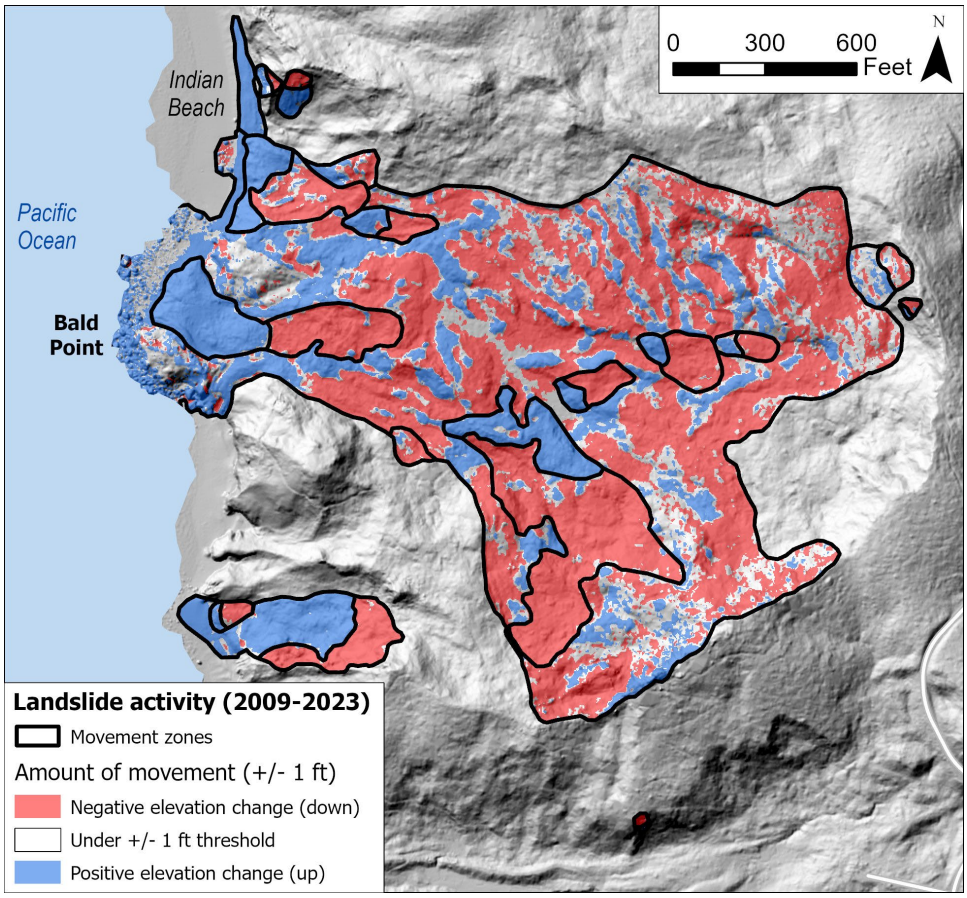

3.5 Canyon Creek Landslide (Indian Beach Road)

The Canyon Creek Landslide is also mapped a historic deep rockslide/rotational landslide and earth flow (e.g., Ecola Point Landslide; **Figure 1-6**; Plate 3). The landslide toe is along Canyon Creek and appears to experience erosion by Canyon Creek. There are three areas of reactivation along the toe of the Canyon Creek Landslide (**Figure 3-7**). Two shallow landslides (landslide toe/bank sloughing) were identified by the serial lidar change mapping. These two areas are located directly along Canyon Creek. As Canyon Creek continues to erode the toe of the Canyon Creek Landslide, episodic landslide toe/bank sloughing will continue. This process results in loss of resisting-force regions of the landslide that promotes continued future landslide reactivation. The third active area is larger and has caused damage to Indian Beach Road. Our research shows this landslide was active in 1982, 2016, and we noted fresh open tension cracks directly above the road during the field work portion of this project in August 2024. The reactivated portions of this landslide are mapped as *Active* and the rest of the landslide is mapped as *High* on the landslide susceptibility/risk map (Plate 6). Unfortunately, critical infrastructure (the only public road to and from Indian Beach) crosses the lower portion of this landslide. This road has been damaged in the past and will likely be damaged again in the future as the process continues, unless this process is mitigated or avoided.

Figure 3-7. Topographic map and cross section of the Canyon Creek Landslide along Indian Beach Road. The central northern portion of this landslide is currently active. Recent landslide movement areas were identified in the serial lidar change analysis (2009–2023) along the toe.

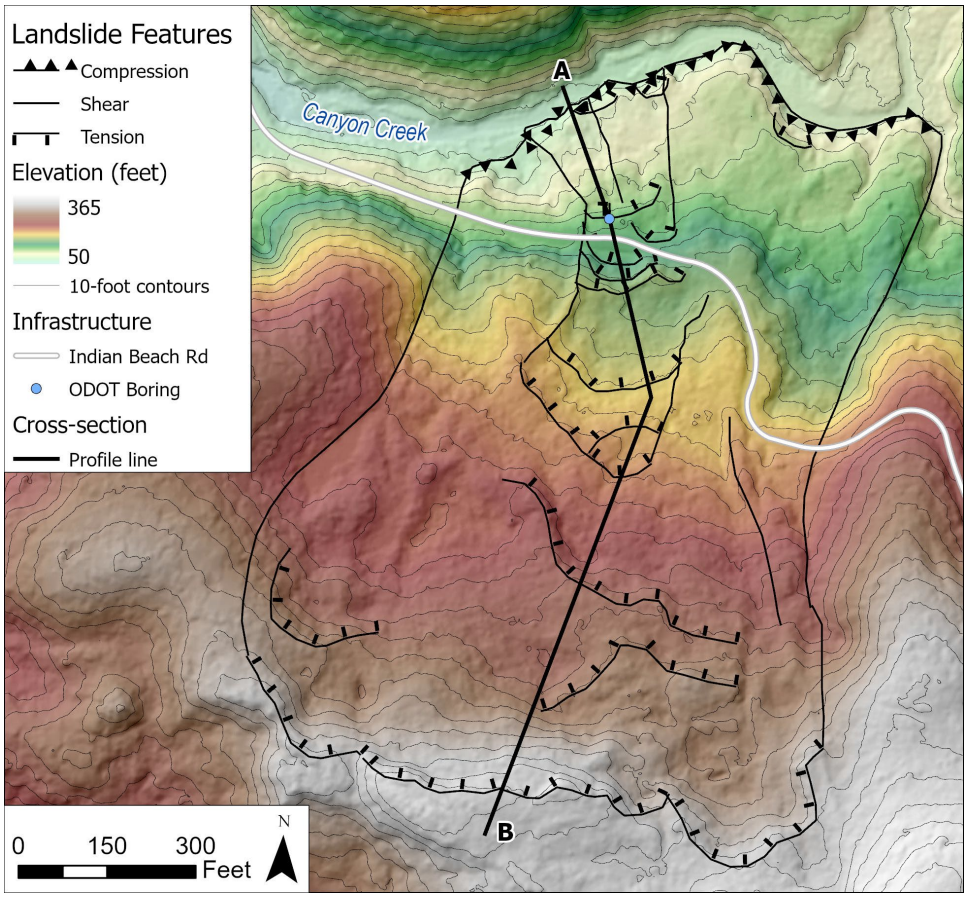

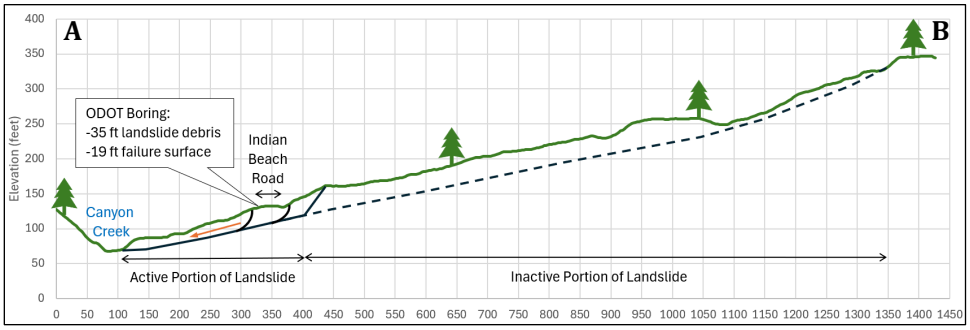

4.0 DISCUSSION AND RECOMMENDATIONS

When planning future development within the study area, for example, expansion or relocation of existing roads, new roads, infrastructure improvements, and grading or stormwater control, use the landslide inventory and susceptibility/risk map created in this project to identify areas of increased landslide potential and follow recommendations for future development. If landslide issues are identified and considered as part of the design phase of the project, the result should be an increase in slope stability and a decrease in risk.

While performing this study, we noted several landslides that have significant enough risk to warrant further investigation (Plate 2, Plate 3, Plate 4, Plate 5, and Plate 6). These include the Ecola Park Road, Ecola Point, and Canyon Creek landslides. If mitigation of any of these landslides is considered, detailed geotechnical evaluation, including borings below the failure surface, monitoring and analysis of groundwater conditions, pre- and post-construction slope stability analysis, and geotechnical design should be performed.

With accurate GIS data for the entire study area, landslide monitoring is a potential next step. Landslide monitoring provides quantitative data that are essential for the evaluation of remediation alternatives, including engineered solutions. The two primary ways to accomplish landslide monitoring are regional and on-the-ground, site-specific techniques. We recommend both. A regional approach might include collecting new lidar datasets and performing change analysis similar to what was performed in this project. This type of regional analysis could be performed periodically (e.g., every five years) and would help OPRD understand which large landslides are moving. This should be coupled with on-the-ground, site-specific monitoring. Current practices include standard surveying and resurveying of markers, serial ground-based lidar scanning, and installation of inclinometers and extensometers. Acoustic-flow monitor (AFM) seismometers can automatically detect movement. For example, the U.S. Geological Survey Cascade Volcano Observatory has a system using AFMs on Mount Rainier (http://volcanoes.usgs.gov/activity/methods/hydrologic/lahardetection.php).

Another form of proactive risk reduction is to review park infrastructure maintenance practices considering the new landslide information. For example, repeated placement of fill can unknowingly add driving force, contributing to continued slope instability, especially in conditions where existing landslides may be only marginally stable. The placement of storm debris and/or soil in the wrong location, for example, near the heads of existing landslides, can also unknowingly cause slope failure simply by adding more weight to the slope. Finally, stormwater runoff routing must be done carefully so that water is not directed onto or into unstable slope areas. Keeping good records of maintenance practices is another way to track effects.

Landslide disasters triggered by large storm events and/or earthquakes should be expected in the future. Preparing for emergency situations, such as storm events and earthquakes can be done in several ways. One can assess the level of readiness and preparedness to deal with a disaster before disaster occurs by estimating damage from specific past hazard events. Landslide data on past events at Ecola, presented in this report, will help OPRD on this task. Another way to prepare is to better understand when these events might be expected. Oregon has a statewide landslide warning system that is initiated by the National Weather Service (NWS) and disseminated by several Oregon state agencies (OEM, ODOT, and DOGAMI). The system could be used by OPRD for monitoring precipitation and resulting slide activity. Knowing when there will be periods of increased landslide potential will help OSP prepare, respond, and recover.

Earthquakes and tsunamis will happen again in the future on the Oregon Coast. The last CSZ earthquake and tsunami was January 26, 1700 (324 years ago; Atwater and others, 2005). Goldfinger and others (2017) estimated the conditional probability of a future earthquake on the CSZ at ~16%–22% in the next 50 years. Because Ecola is on the coast, which is where the CSZ is located, the ground motions during a future CSZ earthquake are likely to be very high. In the future, earthquakes will likely trigger reactivation of existing landslides and create new landslides in the study area. If mitigation of any of the landslides in Ecola is considered, the slope stability analysis pre- and postmitigation design should include the appropriate CSZ seismic loading. We recommend this so the various levels of potential future mitigation (cost) can be compared to the desired dependability (benefit).

Priest and others (2013) created tsunami inundation hazard maps for the entire Oregon Coast. The best way to prepare for the tsunami is to have evacuation routes established with appropriate signage. Gabel and others (2022) created tsunami evacuation maps for the northern Oregon Coast.

Schulz and Wang (2014) analyzed coseismic landslide movement along the northern Oregon Coast and concluded many of the existing active and dormant landslides will reactivate catastrophically during the next CSZ earthquake. They also concluded reactivations of existing landslides may involve feet to tens of yards of movement and that the earthquake will likely trigger the formation of new landslides.

The Sixth Oregon Climate Assessment (Fleishman, 2023) concluded Oregon's average and extreme temperatures will increase, as will related wildfires. Postfire landscapes can increase susceptibility to landslides. Precipitation is projected to increase during winter and decrease during summer, and the number and intensity of heavy winter precipitation events is projected to increase (Fleishman, 2023). The results of the orthophoto analysis show that approximately 21% (1939–1967) to 25% (1995–2000) of the landslides in the study area over the last nearly 100 years occurred during extreme AR storm events like December 1964 (1939–1967) and February 1996 (1995–2000). If climate change results in an increase in the number and intensity of extreme AR storms, the overall frequency of landslides is likely to also increase. There is near certainty that sea level rise will increase in the future as a result of global warming (Fleishman, 2023). Sea level rise can increase coastal erosion, removing resisting-force regions of landslides (toe) and leading to more frequent reactivations. Climate change is primarily driven by increased greenhouse gases. All efforts to decrease the greenhouse gas in our atmosphere will aid in the reduction of climate change.

5.0 CONCLUSIONS

Although we cannot predict when and where the next landslide will occur in Ecola, this report provides datasets covering several different spatial and temporal scales and detailed maps of areas where landslides have occurred. (Plate 3, Plate 4, and Plate 5). From these data and maps, we have created a new landslide susceptibility and risk map (Plate 6) that estimates where future landslide activity may occur and provides recommendations for future development and mitigation. We conclude that the study area has an overall *High* landslide hazard based on the over 270 landslides that cover approximately 21% of the region. In a similar study of the City of Astoria (**Figure 1-1**), 27% of the area within city limits was underlain by existing landslides, which we also determined to be a *High* landslide prone region (Burns and Mickelson, 2013).

We also note that this portion of northwest Oregon has some of the highest average annual precipitation and is susceptible to 24-hour-precipitation-induced debris flows (**Figure 1-2 and Figure 1-9).** The area is also exposed to some of the highest potential ground motions that could occur in response to a megathrust earthquake on the CSZ and is also susceptible to potential shaking from smaller crustal faults that have been identified in the region. Both the high precipitation and potential for large earthquakes are primary triggers for new landslides and reactivation of existing landslides in the future.

Large, deep landslides appear to be the primary threat in Ecola for several reasons. First, deep landslides can impact large areas, leading to significant damage. The size and depth of the deep landslides makes them complicated and potentially very expensive to mitigate, thus, the need for continuing landslide risk management. Landslide risk management can be performed in various ways. We provided discussion and recommendations to OPRD for continued work on landslide risk management. These recommendations are not complete, but they should provide a good foundation.

To have dependable roads, mitigation of landslides under existing roads and redundancy should both be considered. The new landslide maps created as part of this project will help OSP determine where mitigation or redundancy should be implemented. Additional analysis such as cost-benefit analysis maybe required to determine the best future mitigation steps in Ecola.

6.0 ACKNOWLEDGMENTS

Funding for this project was provided by OSP through Interagency Agreement IAA#22- 9312. We thank Matt Rippee, Natural Resource Protection and Sustainability Administrator for the OPRD for initiating this project. We also thank Brady Callahan, GIS Lead, and Ben Cox, Park Manager, Nehalem Bay Management Unit at OPRD. We also thank DOGAMI staff who provided reviews and comments, especially Kaleb Scarberry and Fletcher O'Brien.

7.0 REFERENCES

Atwater, B. F., Musumi-Rokkaku, S., Satake, K., Yoshinobu, T., Kazue, U., Yamaguchi, D. K., 2005, The Orphan Tsunami of 1700–Japanese Clues to a Parent Earthquake in North America. U.S. Geological Survey Professional Paper 1707, United States Geological Survey–University of Washington Press, 146 p., https://pubs.usgs.gov/publication/pp1707, accessed December 23, 2024.

Baksi, A.K., 2022, New $^{40}Ar/^{39}Ar$ ages from the Grande Ronde and Wanapum Basalt, Columbia River Basalt Group (CRBG): Compilation of all ages and relationship to the geomagnetic polarity time scale for ˜17–15 Ma: Journal of Earth System Science, v. 131 158, p. 1-29. https://www.ias.ac.in/article/fulltext/jess/131/0158, accessed December 23, 2024.

Burns, W.J., Coe, J.A., Sener Kaya, B., Ma, L., 2010, Analysis of Elevation Changes Detected from Multi-Temporal LiDAR Surveys in Forested Landslide Terrain in Western Oregon: Environmental and Engineering Geoscience, v. XVI, n. 4, p. 315-341. https://pubs.geoscienceworld.org/aeg/eeg/article-abstract/16/4/315/60383/Analysis-of-Elevation-Changes-Detected-from-Multi?redirectedFrom=fulltext, accessed December 23, 2024.

Burns, W.J., Calhoun, N.C., Roering, J., Sanders, M., Leshchinsky, B., DeSousa, D., Olsen, M., Rengers, F., Mathews, N., in press, Multitemporal Lidar Analysis of Pre and Post Eagle Creek Fire Debris Flows, Western Columbia River Gorge, Hood River and Multnomah Counties, Oregon, Oregon Department of Geology and Mineral Industries, Special Paper 55.

Burns, W.J. and Mickelson, K.A., 2013, Landslide Inventory, Susceptibility Maps, and Risk Analysis for the City of Astoria, Clatsop County, Oregon: Oregon Department of Geology and Mineral Industries Open-File Report O-13-05, GIS data, 33 p. https://pubs.oregon.gov/dogami/ofr/p-O-13-05.htm, accessed December 23, 2024.

Burns, W.J., and Mickelson, K.A., 2016, Protocol for deep landslide susceptibility mapping: Oregon Department of Geology and Mineral Industries Special Paper 48, 66 p., https://pubs.oregon.gov/dogami/sp/p-SP-48.htm, accessed December 23, 2024.

Burns, W.J., Madin, I.P., Mickelson, K.A., 2012, Protocol for shallow-landslide susceptibility mapping: Oregon Department of Geology and Mineral Industries Special Paper 45, 32 p. https://pubs.oregon.gov/dogami/sp/p-SP-45.htm, accessed December 23, 2024.

Burns, W.J., Madin, I.P., and Calhoun, N.C. 2021, Landslide Inventory Map of the Coastal Portion of Clatsop County, Oregon: Oregon Department of Geology and Mineral Industries Open-File Report O-21-10, 1 map plate, scale 1:32,000, Esri™ geodatabase, metadata, https://pubs.oregon.gov/dogami/ofr/O-21-10/OFR-21-10.htm, accessed December 23, 2024.

Burns, W. J., and Madin, I. P., 2009, Protocol for inventory mapping of landslide deposits from light detection and ranging (lidar) imagery: Oregon Department of Geology and Mineral Industries Special Paper 42, 30 p., Esri™ geodatabase template, https://pubs.oregon.gov/dogami/sp/p-SP-42.htm, accessed December 23, 2024.

Burns, W. J., 2007, Comparison of remote sensing datasets for the establishment of a landslide mapping protocol in Oregon: Association of Environmental and Engineering Geologists Special Publication 23, Vail, Colorado, Conference Presentations, 1st North American Landslide Conference.

Calhoun, N.C., Burns, W.J., Franczyk, J.J., 2020, Landslide hazard and risk study of Tillamook County, Oregon, Oregon Department of Geology and Mineral Industries Open-File Report O-20-13, 44 p., Esri™ geodatabase, metadata, https://pubs.oregon.gov/dogami/ofr/p-O-20-13.htm, accessed December 23, 2024.

Camp, V.E., and Wells, R.E., 2021, The case for a long-lived and robust Yellowstone Hotspot: Geological Society of America GSA Today, v. 31, no. 1, p 4-10. https://www.geosociety.org/GSA/Publications/GSA_Today/GSA/GSAToday/science/G477A/article.aspx, accessed November, 21, 2024.

Carson, R. J., and Hankel, H. W., 1975, The 1975 landslide at Ecola State Park, Clatsop County, Oregon: Proceedings of the Oregon Academy of Science, v. 11, p. 86.

Cornforth, D. H., 2005, Landslides in practice: Investigation, analysis, and remedial/preventative options in soils: Hoboken, N. J., John Wiley and Sons, p. 596.

Cressy, F.B., Jr., 1974, Stratigraphy and sedimentation of the Neahkahnie Mountain-Angora Peak area, Tillamook and Clatsop counties, Oregon: Corvallis, Oregon, Oregon State University M.S. thesis, 148 p, 2 plates, scale 1:62,500, cross sections, https://ir.library.oregonstate.edu/concern/graduate_thesis_or_dissertations/9g54xp14g?locale=en, accessed December 23, 2024.

Fleishman, E., editor. 2023. Sixth Oregon Climate Assessment. Oregon Climate Change Research Institute, Oregon State University, Corvallis, Oregon, https://blogs.oregonstate.edu/occri/oregon-climate-assessments, accessed December 23, 2024.

Gabel, L. L. S., Allan, J. C., and O'Brien, F. E., 2022, Tsunami Evacuation Analysis of Cannon Beach, Arch Cape, and Falcon Cove, Clatsop County, Oregon: Oregon Department of Geology and Mineral Industries Open-File Report O-22-02, 39 p., Esri™ geodatabase, metadata, https://pubs.oregon.gov/dogami/ofr/O-22-02/p-O-22-02.htm, accessed December 23, 2024.

Goldfinger, C., Galer, S., Beeson, J., Hamilton, T., Black, B., Romsos, C., Patton, J., Nelson, C. H., Hausmann, R., and Morey, A., 2017, The importance of site selection, sediment supply, and hydrodynamics: A case study of submarine paleoseismology on the northern Cascadia margin, Washington USA: Marine Geology, v. 384, p. 4-16, 17, 25-46, https://www.sciencedirect.com/science/article/abs/pii/S0025322716301220?via%3Dihub, accessed December 23, 2024.

Highland, L., compiler, 2004, Landslide types and processes, U.S. Geological Fact Sheet 2004-3072 (ver. 1.1), 4 p., https://pubs.usgs.gov/fs/2004/3072/, accessed December 23, 2024.

Kasbohm, J., and Schoene, B., 2018, Rapid eruption of the Columbia River flood basalt and correlation with mid-Miocene climate optimum; Science Advances, v. 4, no. 9. https://advances.sciencemag.org/content/4/9/eaat8223, accessed December 23, 2024.

Kasbohm, J., Schoene, B., Mark, D.F., Murray, J., Reidel, S., Szymanowski, D., Barfod, D., Barry, T., 2023, Eruption history of the Columbia River Basalt Group constrained by high-precision U-Pb and $^{40}Ar/^{39}Ar$ geochronology: Earth and Planetary Science Letters, Volume 617, p. 1-14. https://www.sciencedirect.com/science/article/abs/pii/S0012821X23002820, accessed December 23, 2024.

Keefer, D. K. and Johnson, A.M., 1983, Earth Flows: Morphology, Mobilization, and Movement, U.S. Geological Survey, Professional Paper 1264, 61 p., 3 map plates, scales 1:200,1:6,000, 1:750,000, https://pubs.usgs.gov/publication/pp1264, accessed December 23, 2024.

Lewis, M., Clark, W., and Members of the Corps of Discovery. (2002). January 8 & 10, 1806. In G. Moulton (Ed.), The Journals of the Lewis and Clark Expedition. Lincoln: University of Nebraska Press. Retrieved Oct. 1, 2005, from the University of Nebraska Press / University of Nebraska-Lincoln Libraries-Electronic Text Center, The Journals of the Lewis and Clark Expedition web site: https://lewisandclarkjournals.unl.edu/item/lc.jrn.1806-01-10#lc.jrn.1806-01-10.01 https://lewisandclarkjournals.unl.edu/item/lc.jrn.1806-01-08#lc.jrn.1806-01-08.03

Madin, I.P., 2009, Oregon: A Geologic History, Oregon Department of Geology and Mineral Industries, Interpretive Map Series 28, 1 map plate, scale 1:633,600, https://pubs.oregon.gov/dogami/ims/p-ims-028.htm, accessed December 23, 2024.

Madin, I.P., Francyzk, J.J., Bauer, J.M., Azzopardi, C.J., 2021, Oregon Seismic Hazard Database: Oregon Department of Geology and Mineral Industries Digital Data Series (OSHD) release 1.0, 48 p. 3 map plates, scale 1:825,000, Esri™ geodatabase, https://pubs.oregon.gov/dogami/dds/p-OSHD-1.htm, accessed December 23, 2024.

Neel, R.H., 1976, Geology of the Tillamook Head-Necanicum Junction area, Clatsop County, northwest Oregon: Corvallis, Oregon, Oregon State University M.S. Thesis, 204 p, 2 plates, scale 1:62,500, cross sections, https://ir.library.oregonstate.edu/concern/graduate_thesis_or_dissertations/9w0327611?locale=en, accessed December 23, 2024.

Niem, A. R., 1975, Geology of Hug Point State Park Northern Oregon Coast: The Ore Bin, v. 37, no. 2, p. 17-36, https://pubs.oregon.gov/dogami/og/OBv37n02.pdf, accessed December 23, 2024.

Niem, A.R., and Cressy, F.B., Jr., 1973, K-Ar dates from the Neahkahnie Mountain and Tillamook Head areas of northwestern Oregon coast: Isochron/West, v. 7, no. 3, p. 13-15, https://geoinfo.nmt.edu/publications/periodicals/isochronwest/7/iw_v07_p13.pdf, accessed December 23, 2024.

Niem, A. R., and Niem, W. A., 1985, Oil and gas investigation of the Astoria Basin, Clatsop and Northernmost Tillamook Counties, Northwest Oregon: Oregon Department of Geology and Mineral Industries Oil and Gas Investigation OGI-14, 1 map plate, scale 1:100,000, https://pubs.oregon.gov/dogami/ogi/OGI-14.pdf, accessed December 23, 2024.

Niem, A.R., McKnight, B.K., and Meyer, H.J., 1994, Sedimentary, volcanic, and tectonic framework of forearc basins and the Mist Gas Field, northwest Oregon, *in* Swanson, D.A., and Haugerud, R.A., eds., Geologic field trips in the Pacific Northwest: Geological Society of America 106th Annual Meeting, Department of Geological Sciences, University of Washington, p. 1F1-1F42-774.

Niem, A.R., Snavely, P.D., Jr., and Niem, W.A., 1990, Onshore-offshore geologic cross sections from the Mist Gas Field, northern Oregon Coast Range to the northwest Oregon continental shelf and slope: Oregon Department of Geology and Mineral Industries Oil and Gas Investigation 17, 1 map plate, scale 1:100,000, 46 p, https://pubs.oregon.gov/dogami/ogi/OGI-17.pdf, accessed December 23, 2024.

Niem, A.R., Van Atta, R.O., Livingston, V.E., Jr., and Rau, W.W., 1973, Cenozoic geology of northwestern Oregon and adjacent southwestern Washington, in Beaulieu, J.D., ed., Geologic field trips in northern Oregon and southern Washington: Oregon Department of Geology and Mineral Industries Bulletin 77, p. 93-132, pubs.oregon.gov/dogami/B/B-077.pdf, accessed November 21, 2024.

North, W. B., and Byrne, J. V., 1965, Coastal landslides of northern Oregon: The Ore Bin, v. 27, no. 11, p. 217-241. https://pubs.oregon.gov/dogami/og/OBv27n11.pdf, accessed November 21, 2024.

NV5 Geospatial, 2023, OLC Ecola State Park, Oregon Lidar 2023 Technical Data Report.

NWS, Public Information Statement, December 4, 2007.

Pfeiffer, T., 2016, Phase 1 – Landslide Reconnaissance Memorandum, Foundation Engineering, Inc.

Priest, G. R., Witter, R. C., Y. Zhang, Y., Wang, K., Goldfinger, C., Stimely, L. L., English, J. T., Pickner, S. G., Hughes, K. L. B., Wille, T. E., and Smith, R. L., 2013, Tsunami inundation scenarios for Oregon: Oregon Department of Geology and Mineral Industries Open-File Report O-13-19, 14 p., GIS data. https://pubs.oregon.gov/dogami/ofr/p-O-13-19.htm, accessed December 23, 2024.

Reidel, S.P., Johnson, V.G., and Spane, F.A., 2002, Natural gas storage in basalt aquifers of the Columbia Laboratory, Basin, Pacific Northwest USA: a guide to site characterization: Richland, Wash., Pacific Northwest National 277 p. https://www.pnnl.gov/main/publications/external/technical_reports/PNNL-13962.pdf, accessed December 23, 2024.

Reidel, S.P., and Tolan, T.L., 2013, The Grande Ronde Basalt, Columbia River Basalt Group, *in* Reidel, S.P., Camp, V.E., Martin, M.E., Ross, M.E., Wolff, J.A., Martin, B.S., Tolan, T.L., and Wells, R.E., eds., The Columbia River Flood Basalt Province: Boulder, Colorado, Geological Society of America Special Paper 497, p. 117-154. https://pubs.geoscienceworld.org/books/book/661/chapter-abstract/3807152/The-Grande-Ronde-Basalt-Columbia-River-Basalt?redirectedFrom=fulltext, accessed December 23, 2024.

Schaefer, M. G., Barker, B. L., Taylor, G. H., and Wallis, J. R., 2008, Regional precipitation-frequency analysis and spatial mapping of 24-hour precipitation for Oregon: Oregon Department of Transportation Research Unit, Research Report SPR 656 (OR-RD-FHWA-08-05), 63 p. plus appendices, https://www.oregon.gov/ODOT/Programs/ResearchDocuments/SPR656_Rainfall_Analysis_Final_Report_web.pdf, accessed December 23, 2024.

Schlicker, H. G., Corcoran, R. E., and Bowen, R. G., 1961, Geology of the Ecola State Park landslide area, Oregon: The Ore Bin, v. 23, no. 9, p. 85-90. https://pubs.oregon.gov/dogami/og/OBv23n09.pdf, accessed December 23, 2024.

Schlicker, H. G., Deacon, R. J., Beaulieu, J. D., and Olcott, G. W., 1972, Environmental geology of the coastal region of Tillamook and Clatsop Counties, Oregon: Oregon Department of Geology and Mineral Industries Bulletin 74. https://pubs.oregon.gov/dogami/B/B-074.zip, accessed December 23, 2024.

Snavely, P.D., Jr., MacLeod, N.S., Wagner, H.C., and Rau, W.W., 1976, Geologic map of the Cape Foulweather and Euchre Mountain quadrangles, Lincon County, Oregon: U.S. Geological Survey Miscellaneous Investigation Series Map I-868, 1 map plate, scale 1:62,500, https://pubs.usgs.gov/publication/i868, accessed November 21, 2024.

Schulz, W. H., and G. Wang, 2014, Residual shear strength variability as a primary control on movement of landslides reactivated by earthquake-induced ground motion: Implications for coastal Oregon, U.S., Journal of Geophysical Research: Earth Surface, v. 119, no. 7, https://agupubs.onlinelibrary.wiley.com/doi/10.1002/2014JF003088, accessed December 23, 2024.

Tardif, M., 2023, Ecola State Park – Geotechnical Memorandum: Oregon Department of Transportation, Geo/Hydro/Hazmat Unit, memorandum to Oregon Parks and Recreation Department, 8 p.

Tolan, T.L., Martin, B.S., Reidel, S.P., Anderson, J.L., Lindsey, K.A., and Burt, W., 2009a, An introduction to the stratigraphy, structural geology, and hydrogeology of the Columbia River flood-basalt province: A primer for the GSA CRBG field trips, in O'Connor, J. E., Dorsey, R. J., and Madin, I. P., eds., Volcanoes to vineyards: geologic field trips through the dynamic landscape of the Pacific Northwest: Geological Society of America Field Guide 15, p. 599-643. https://pubs.geoscienceworld.org/books/book/885/chapter/3931355/An-introduction-to-the-stratigraphy-structural, accessed December 23, 2024.

Tolan, T.L., Reidel, S.P., Beeson, M.H., Anderson, J.L., Fecht, K.R., and Swanson, D.A., 1989, Revisions to the estimates of the areal extent and volume of the CRBG, *in* Reidel, S. P., and Hooper, P. R., eds., Volcanism and tectonism in the Columbia River Flood-Basalt Province: Geological Society of America Special Paper 239, p. 1-20. https://pubs.geoscienceworld.org/books/book/375/chapter/3796993/Revisions-to-the-estimates-of-the-areal-extent-and, accessed December 23, 2024.

Turner, A. K., and Schuster, R. L., eds., 1996, Landslides: Investigation and Mitigation: Washington, D.C., National Research Council, Transportation Research Board Special Report 247, 673 p, https://onlinepubs.trb.org/Onlinepubs/sr/sr247/sr247.pdf, accessed December 23, 2024.

U.S. Army Corps of Engineers, 1939, 1967, 1975, Aerial photographs of the Oregon coast.

U.S. Department of Agriculture, 1995, 2000, 2005, 2009, 2011, 2012, 2014, 2016, 2018, 2020, 2022: NAIP Digital Ortho Photo Images. Oregon Statewide Imagery Program (OSIP).

U.S. Geological Survey National Cooperative Geologic Mapping Program, 2020, GeMS (Geologic Map Schema)—A standard format for the digital publication of geologic maps: U.S. Geological Survey Techniques and Methods, book 11, chap. B10, 74 p., https://pubs.usgs.gov/publication/tm11B10, accessed December 23, 2024.

Varnes, D. J., 1978, Slope movement types and processes, in Schuster, R. L., and Krizek, R. J., eds., Landslides—Analysis and control: Washington, D.C., Transportation Research Board Special Report 176, p. 11–33, https://onlinepubs.trb.org/Onlinepubs/sr/sr176/176-002.pdf, accessed December 23, 2024.

Watershed Sciences, 2009, Lidar remote sensing data collection Department of Geology and Mineral Industries Oregon North Coast, https://pubs.oregon.gov/dogami/ldq/reports/North_Coast_Lidar_Report_2009.pdf, accessed December 23, 2024.

Wavra, Bryan, 2021. Budgetary Proposal for Slope Stabilization of the North Slide at Ecola State Park, GeoStabilization International.

Wells, R.E., Niem, A.R., Evarts, R.C., and Hagstrum, J.T., 2009, The Columbia River Basalt Group-From the gorge to the sea; *in* O'Connor, J.E., Dorsey, R.J., and Madin, I.P., eds., Volcanoes to Vineyards: Geologic Field Trips through the Dynamic Landscape of the Pacific Northwest: Geological Society of America Field Guide 15, p. 737-774, https://pubs.geoscienceworld.org/gsa/books/edited-volume/885/chapter-abstract/3932152/The-Columbia-River-Basalt-Group-From-the-gorge-to?redirectedFrom=fulltext, accessed November 21, 2024.

Wells, R.E., Bentley, R.D., Beeson, M.H., Mangan, M.T., and Wright, T.L., 1989, Correlation of Miocene flows of the Columbia River Basalt from the central Columbia River Plateau to the coast of Oregon and Washington, in Reidel, S.P. and Hooper, P.R., eds., Volcanism and tectonism in the Columbia River flood-basalt province, Geological Society of America Special Paper 239, p. 113-129, https://pubs.geoscienceworld.org/gsa/books/edited-volume/375/chapter-abstract/3797019/Correlation-of-Miocene-flows-of-the-Columbia-River?redirectedFrom=fulltext, accessed November 21, 2024.

Wells, R.E., Haugerud, R.A., Niem, A.R., Niem, W.A., Ma, L., Evarts, R..C., O'Connor, J.E., Madin, I.P., Sherrod, D.R., Beeson, M.H., Tolan, T.L., Wheeler, K.L., Hanson, W.B., and Sawlan, M.G., 2020, Geologic map of the greater Portland metropolitan area and surrounding region, Oregon and Washington: U.S. Geological Survey Scientific Investigations Map 3443, 4 map plates, Esri™ geodatabase, metadata, 55 p., https://pubs.usgs.gov/publication/sim3443, accessed December 23, 2024.

Wolfe, E.W., and McKee, E.H., 1968, Geology of the Grays River quadrangle, Wakhiuakum and Pacific Counties, Washington: Washington Division of Mines and Geology Geologic Map GM-4, https://www.dnr.wa.gov/publications/ger_gm4_geol_graysriver_62k.pdf, accessed November 21, 2024.

Wiley, T. J., 2000, Relationship between rainfall and debris flows in western Oregon: Oregon Geology, v. 62, no. 2, p. 27–34, 39–43, https://pubs.oregon.gov/dogami/og/OGv62n02.pdf, accessed December 23, 2024.

Witter, R. C., Horning, T., and Allan, J. C., 2009, Coastal erosion hazard zones in southern Clatsop County, Oregon: Seaside to Cape Falcon: Oregon Department of Geology and Mineral Industries Open-File Report O-09-06, 39 p. with appendices, GIS files, https://pubs.oregon.gov/dogami/ofr/O-09-06.zip, accessed December 23, 2024.